Received: 19 September 2018 | Revised: 11 June 2019 | Accepted: 13 June 2019

DOI: 10.1111/bre.12381

ORIGINAL ARTICLE

Basin Research | IAS EAGE | WILEY

The Tajik Basin: A composite record of sedimentary basin evolution in response to tectonics in the Pamir

James B. Chapman[1] | **Barbara Carrapa**[2] | **Peter G. DeCelles**[2] | **James Worthington**[3] | **Nicoletta Mancin**[4] | **Miriam Cobianchi**[4] | **Marius Stoica**[5] | **Xin Wang**[6] | **Mustafo Gadoev**[7] | **Ilhomjon Oimahmadov**[7]

[1]Department of Geology and Geophysics, University of Wyoming, Laramie, Wyoming

[2]Department of Geosciences, University of Arizona, Tucson, Arizona

[3]Division of Geological and Planetary Sciences, California Institute of Technology, Pasadena, California

[4]Department of Earth and Environment Sciences, University of Pavia, Pavia, Italy

[5]Department of Geology, Bucharest University, Bucharest, Romania

[6]Key Laboratory of Western China's Environmental Systems, Lanzhou University, Lanzhou, China

[7]Institute of Geology, Earthquake Engineering and Seismology, Tajik Academy of Sciences, Dushanbe, Tajikistan

Correspondence
James B. Chapman, Department of Geology and Geophysics, University of Wyoming, Laramie, WY 82071.
Email: jay.chapman@uwyo.edu

Funding information
Directorate for Geosciences, Grant/Award Number: EAR-1450899

Abstract

Investigation of a >6-km-thick succession of Cretaceous to Cenozoic sedimentary rocks in the Tajik Basin reveals that this depocentre consists of three stacked basin systems that are interpreted to reflect different mechanisms of subsidence associated with tectonics in the Pamir Mountains: a Lower to mid-Cretaceous succession, an Upper Cretaceous–Lower Eocene succession and an Eocene–Neogene succession. The Lower to mid-Cretaceous succession consists of fluvial deposits that were primarily derived from the Triassic Karakul–Mazar subduction–accretion complex in the northern Pamir. This succession is characterized by a convex-up (accelerating) subsidence curve, thickens towards the Pamir and is interpreted as a retroarc foreland basin system associated with northward subduction of Tethyan oceanic lithosphere. The Upper Cretaceous to early Eocene succession consists of fine-grained, marginal marine and sabkha deposits. The succession is characterized by a concave-up subsidence curve. Regionally extensive limestone beds in the succession are consistent with late stage thermal relaxation and relative sea-level rise following lithospheric extension, potentially in response to Tethyan slab rollback/foundering. The Upper Cretaceous–early Eocene succession is capped by a middle Eocene to early Oligocene (ca. 50–30 Ma) disconformity, which is interpreted to record the passage of a flexural forebulge. The disconformity is represented by a depositional hiatus, which is 10–30 Myr younger than estimates for the initiation of India–Asia collision and overlaps in age with the start of prograde metamorphism recorded in the Pamir gneiss domes. Overlying the disconformity, a >4-km-thick upper Eocene–Neogene succession displays a classic, coarsening upward unroofing sequence characterized by accelerating subsidence, which is interpreted as a retro-foreland basin associated with crustal thickening of the Pamir during India–Asia collision. Thus, the Tajik Basin provides an example of a long-lived composite basin in a retrowedge position that displays a sensitivity to plate margin processes. Subsidence, sediment accumulation and basin-forming mechanisms are influenced by subduction dynamics, including periods of slab-shallowing and retreat.

KEYWORDS

basin subsidence, foreland basins, geodynamics, stratigraphy, subduction-related basins, tectonics and sedimentation

1 | INTRODUCTION

The modern Tajik Basin is a foreland basin related to flexural loading by the Pamir Mountains to the east and by the westernmost Tian Shan Mountains to the north and west (Burtman & Molnar, 1993) (Figure 1a). Traditionally, foreland basin sedimentation in the Tajik Basin is regarded to have started during the Late Oligocene to Early Miocene, consistent with the onset of rapid subsidence and deposition of large volumes of coarse-grained clastic deposits (Klocke et al., 2017; Leith, 1982, 1985; Nikolaev, 2002; Varentsov, Aleshina, & Kornienko, 1977). However, Carrapa et al. (2015) suggested that a foreland basin

Highlights

- The Cretaceous to Cenozoic Tajik Basin consists of three stacked basin systems.
- The Lower Cretaceous succession is as a retroarc foreland basin system associated with subduction of oceanic lithosphere.
- The Upper Cretaceous to early Eocene succession is an extensional basin related to slab rollback.
- The Eocene–Neogene succession is a retro-foreland basin associated with India–Asia collision.

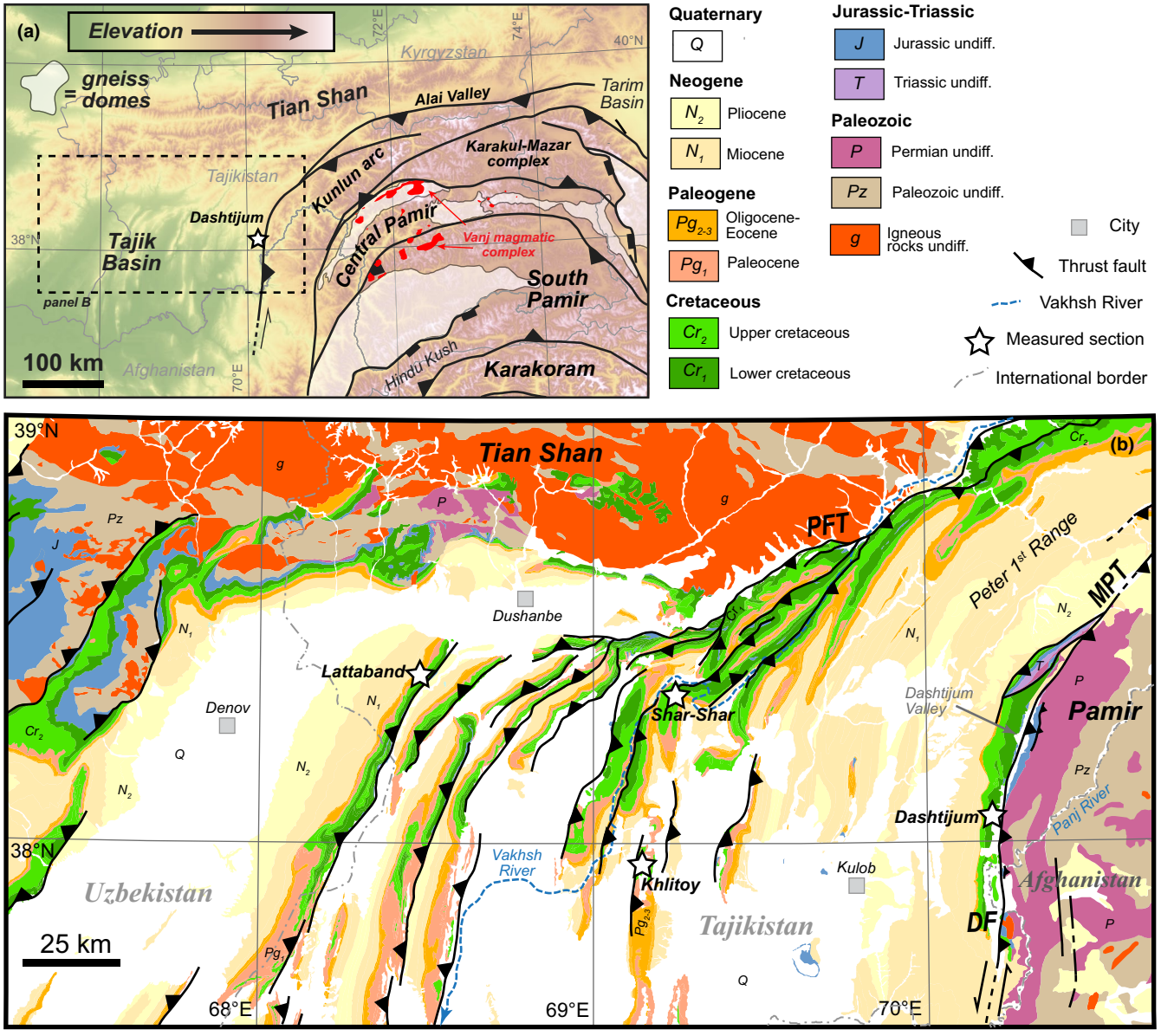

FIGURE 1 (a) Overview map of the Pamir Mountains and Tajik Basin. (b) Geologic map of the Tajik Basin-modified from Vlasov et al. (1991)

system was in place by the Middle Eocene and Hamburger, Sarewitz, Pavlis, and Popandopulo (1992) suggested that the foreland basin system initiated during the Late Jurassic to Early Cretaceous. The timing of initial foreland basin sedimentation in the Tajik Basin is important because it is one of the primary geological indicators for the timing of shortening, crustal thickening and uplift of the Pamir Mountains and is used to reconstruct the tectonic and paleoclimatic evolution of the region (Bosboom et al., 2013, 2017; Burtman & Molnar, 1993; Carrapa et al., 2015; Nikolaev, 2002).

Obfuscating the question of foreland basin initiation is a ≥3-km-thick succession of Jurassic to lower Paleogene sedimentary rocks in the Tajik Basin that is commonly referred to as the "pre-orogenic" sequence (e.g. Nikolaev, 2002). Basin models previously proposed for these strata include: a cratonic basin, passive margin, back-arc basin, peripheral foreland basin and retroarc foreland basin (Bratash, Egupov, Pechnikov, & Shelomentsev, 1970; Burtman, 2000; Burtman & Molnar, 1993; Carrapa et al., 2015; Chatelain, Roecker, Hatzfeld, & Molnar, 1980; Hamburger et al., 1992; Leith, 1985; Nikolaev, 2002; Sengor, 1984; Tapponnier, Mattauer, Proust, & Cassaigneau, 1981; Tevelev & Georgievskii, 2012; Ulmishek, 2004; Varentsov et al., 1977; Zonenshain, 1990). The wide variety of interpretations for a single basin suggests the possibility that the basin evolved in response to multiple tectonic mechanisms.

The goals of this study are to constrain the Mesozoic through Cenozoic stratigraphic and sedimentological record of the Tajik Basin, better resolve the nature of Jurassic–lower Paleogene sedimentation, place the basin in an actualistic tectonic context and relate the basin history to the orogenic evolution of the Pamir Mountains. To accomplish this, four stratigraphic sections (Figure 1b) were measured across the Tajik Basin and detailed sedimentological, geochronological, petrological, paleontological and subsidence analyses were undertaken on the easternmost (most proximal to the Pamir), and most complete, measured section.

2 | GEOLOGIC SETTING

2.1 | The Tian Shan and Pamir Mountains

The westernmost Tian Shan is part of the Central Asian Orogenic Belt and is chiefly comprised of Permian igneous and metamorphic rocks associated with the Gissar arc and by late Paleozoic metavolcanic and metasedimentary rocks associated with the Zaravshan subduction–accretion complex (Figure 1b) (Käßner et al., 2016; Worthington et al., 2017). Uplift and erosion of the western Tian Shan began during the early Miocene and has accelerated since ca. 10 Ma (DeGrave et al., 2012; Jepson et al., 2018; Käßner et al., 2016).

The Pamir Mountains are the westernmost part of the Tibetan Plateau and are composed of terranes that were constructed on or accreted to the southern margin of Asia during the late Paleozoic to early Mesozoic, including the Kunlun arc, Karakul–Mazar subduction–accretion complex, Central Pamir terrane and South Pamir terrane (Figure 1a) (Burtman & Molnar, 1993; Robinson, Ducea, & Lapen, 2012; Schwab et al., 2004). The Kunlun arc was built on the southern edge of the Tajik–Tarim continent and is composed primarily of Late Devonian to Early Permian plutons and volcaniclastic metasedimentary rocks (Schwab et al., 2004; Xiao, Windley, Chen, Zhang, & Li, 2002). The Karakul–Mazar subduction–accretion complex was constructed outboard of the Kunlun arc and is composed of Triassic metasedimentary and metavolcanic mélange extensively intruded by 230–210 Ma intermediate igneous rocks (Robinson et al., 2012, 2007; Schwab et al., 2004). Thermochronological data from the Kunlun arc and Karakul–Mazar complex indicate moderate (<10 km) exhumation since the Triassic, with pulses of exhumation during the mid-Cretaceous, Paleocene to early Eocene and Early Miocene (Robinson et al., 2004, 2007; Schmalholz, 2004; Sobel et al., 2013).

The Central Pamir and South Pamir terranes are composed of a metamorphosed Paleozoic–Triassic passive margin sequence overlain by upper Mesozoic marine to continental sedimentary rocks (Rutte et al., 2017; Schwab et al., 2004). Major igneous complexes in the Central and South Pamir terranes include the South Pamir batholith (120–100 Ma), Upper Cretaceous mafic magmatism (80–70 Ma) and the Vanj magmatic complex (45–35 Ma) (Chapman, Scoggin, et al., 2018; Schmalholz, 2004) (Figure 1a). Shortening is concentrated at the outer margin of the Pamir and in the Tajik fold–thrust belt, which is a thin-skinned, bivergent fold–thrust belt that propagated from both the Pamir and the Tian Shan into the Tajik Basin beginning in the Early Miocene (Chapman et al., 2017).

2.2 | Origin of the late Jurassic—Early Paleogene Tajik Basin

Several contrasting basin models have been proposed to explain the late Jurassic to early Paleogene Tajik Basin. A cratonic basin (also termed intracratonic or sag basin) is the most widely cited origin for the Mesozoic Tajik Basin (Burtman, 2000; Burtman & Molnar, 1993; Nikolaev, 2002; Schneider et al., 2013; Ulmishek, 2004). This basin classification originated in the Soviet literature (Bratash et al., 1970; Varentsov et al., 1977) and largely predates modern basin classification schemes (e.g. Ingersoll, 2012). Burtman and Molnar (1993) suggested that Paleozoic shortening and crustal thickening of the Tajik microcontinent resulted in a high plateau that may have collapsed by crustal extension during the Triassic. They proposed that following extension, the basin subsided thermally from the Jurassic until the Late Oligocene to Early Miocene.

Thermal subsidence since the mid-Mesozoic was also proposed by Leith (1982, 1985), who suggested that the concave-up shape of the subsidence curve during the Cretaceous is indicative of crustal stretching. Leith (1985) proposed that the Mesozoic to Early Miocene Tajik Basin originated as a passive margin that transitioned southwards into an open ocean. Large changes in the thickness of the Cretaceous section over short distances in the Tajik Basin were used to support a rift margin geometry (Leith, 1985). Subsequent structural studies, however, have shown that the abrupt thinning of Cretaceous strata is a result of thrust displacement in the Tajik thrust belt (Chapman et al., 2017; Hamburger et al., 1992).

Another model for the Mesozoic Tajik Basin is a back-arc basin (Chatelain et al., 1980; Tapponnier et al., 1981; Tevelev & Georgievskii, 2012; Zonenshain, 1990). During the late Paleozoic, north-directed subduction of Paleo-Tethyan oceanic lithosphere occurred along the southern margin of the Tajik–Tarim continent to construct the Kunlun arc (Boulin, 1988; Tapponnier et al., 1981). Triassic extension of the Turan platform and Tajik Basin has been associated with slab rollback or steepening in this subduction system (Brookfield & Hashmat, 2001) and some authors have suggested that extension in the Tajik Basin may have continued into the Cretaceous (Tevelev & Georgievskii, 2012). The back-arc basin model is based largely on regional comparisons to the Black Sea and South Caspian Sea that are underlain by oceanic crust (Zonenshain & Le Pichon, 1986). Recent geophysical studies have shown that the Tajik Basin is underlain by 32–37-km-thick continental crust (excluding sediment thickness, total crustal thickness = 40–45 km) (Schneider et al., 2013; Sippl et al., 2013).

Finally, the Upper Jurassic to lower Paleogene Tajik Basin may be a foreland basin (Carrapa et al., 2015; Hamburger et al., 1992; Sengor, 1984). The southern Asian margin experienced significant deformation during Mesozoic subduction of Tethyan oceanic lithosphere and accretion of continental blocks to the margin (Angiolini, Zanchi, Zanchetta, Nicora, & Vezzoli, 2013; Schwab et al., 2004; Sengor, 1984). Hamburger et al. (1992) noted that sedimentation rates increased during the Late Jurassic to Early Cretaceous in the Tajik Basin and that Cretaceous rocks have a southerly source that may be related to terrane accretion processes (e.g. Cimmerian orogeny; Angiolini et al., 2013) in the interior of the Pamir–Hindu Kush orogenic system. This model suggests that the Mesozoic Tajik basin is a peripheral foreland basin associated with southward underthrusting of Asian crust beneath the Pamir. Similarly, the western Tarim Basin contains thick, uppermost Jurassic to lower Cretaceous coarse clastic deposits that were interpreted by Sobel (1999) to have been deposited in a compressional(?) flexural basin (Sobel, 1999). Early to mid-Cretaceous shortening and crustal thickening have also been reported in the Pamir interior associated with the northward subduction of Tethyan oceanic lithosphere (Chapman, Robinson, et al., 2018; Robinson, 2015). These studies suggest that the Mesozoic Tajik Basin may be a retroarc foreland basin system located inland of the Cretaceous Karakoram/South Pamir continental arc (Chapman, Scoggin, et al., 2018).

2.3 | Stratigraphy of the Tajik Basin

Basement in the Tajik Basin consists of Proterozoic to Paleozoic continental crust that was accreted onto Asia during the late Carboniferous to early Permian (Burtman & Molnar, 1993; Schwab et al., 2004). Carboniferous to Permian igneous and metamorphic rocks associated with this subduction–accretion event are widely exposed in the westernmost Tian Shan Worthington et al., 2017) (Figure 1b). Permian and Triassic sedimentary rocks are locally present on the Tajik Basin margins and are thought to be locally present at depth (Nikolaev, 2002) (Figure 1b).

Basin-wide deposition began during the Jurassic. Lower Jurassic rocks consist of fluvial sandstone, coal and conglomerate (Brookfield & Hashmat, 2001). The middle Jurassic succession is dominated by shallow marine carbonates that thicken southeastwards from 200 to 500 m, which is inferred to be the opening direction of the Jurassic shoreline (Bratash et al., 1970; Ulmishek, 2004). Upper Jurassic rocks transition from carbonate to a several hundred metre-thick evaporite succession that thins abruptly towards the northern margin of the basin (Fürsich, Brunet, Auxiètre, & Munsch, 2017).

Lower Cretaceous rocks consist primarily of nonmarine red sandstone and siltstone, locally interbedded with thin evaporitic layers (Djalilov, 1971). The Lower Cretaceous succession thickens eastwards, from 300 to 600 m in the westernmost Tian Shan to ca. 1.5 km along the Pamir front (Burtman, 2000; Varentsov et al., 1977). Upper Cretaceous rocks in the Tajik Basin record the first of several transgressive–regressive cycles of the Paratethys Sea that connected the Tarim and Tajik Basins (Bosboom et al., 2017). Upper Cretaceous rocks consist primarily of dark grey to green, marine shale, limestone and evaporite (Djalilov, 1971). The Upper Cretaceous succession thickens from 500 to 750 m in the central Tajik Basin to >1 km adjacent the Pamir Mountains (Burtman, 2000). The Cretaceous rocks have been subdivided into many local formations (cf., Burtman, 2000), although most previous workers divided and mapped the succession in terms of Stage names (Vlasov, Yu, Dyakov, & Cherev, 1991) (Figure 2). The Cretaceous succession examined for this study is here subdivided and named the Schuchi-poyon, Hasarak-bolo and Sangoba Formations (Figure 2).

Unlike the Cretaceous stratigraphy, local formation names or regionally correlated subdivision names are commonly used for Cenozoic strata in the Tajik Basin (Burtman, 2000) (Figure 2). Paleocene rocks are lithologically similar

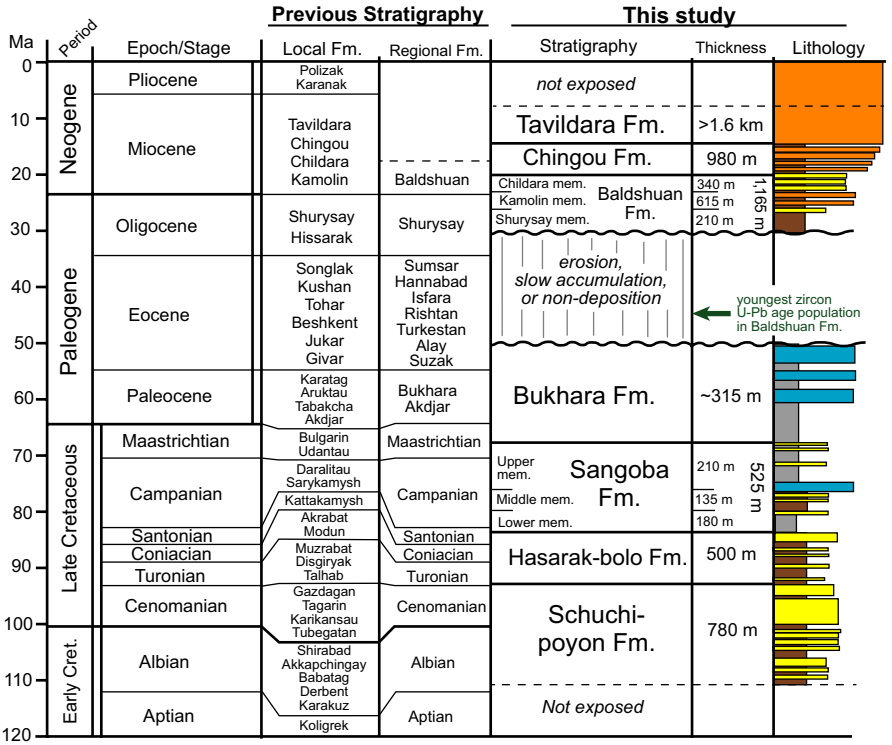

FIGURE 2 Stratigraphic column showing local (within Tajikistan) and regional (correlated across Central Asia) stratigraphic nomenclature (Burtman, 2000; Bosboom et al., 2017; Klocke et al., 2017), and stratigraphic nomenclature employed in this study, which is based on the Dashtijum measured section

to Upper Cretaceous rocks and include shallow marine limestone, calcareous mudstone and minor evaporite (Davidzon, Kreidenkov, & Salibaev, 1982). Thick (≤300 m) limestone beds in the Paleocene section are regionally extensive and known as the Bukhara (or Buhara) Formation (Nikolaev, 2002). The Eocene in the Tajik Basin consists of up to 400 of red to green mudstone interbedded with evaporite, carbonate rocks and sandstone (Bosboom et al., 2017; Davidzon et al., 1982). In many locations the Eocene is partially eroded and separated from the overlying Oligocene and younger section by a regional disconformity to slight angular unconformity (Burtman, 2000; Nikolaev, 2002).

Oligocene and younger rocks in the Tajik Basin are commonly classified as the synorogenic assemblage (Bratash et al., 1970; Burtman & Molnar, 1993; Klocke et al., 2017; Nikolaev, 2002). In general, the ages of the formations in the synorogenic assemblage are poorly constrained (e.g. Klocke et al., 2017). At the base of the synorogenic assemblage is the Oligocene Baldshuan Formation, which is subdivided into the Shurysay, Kamolin and Childara Members (Figure 2). The Shurysay Member consists of ≤300 m of alternating fine-grained red sandstone, mudstone and gypsum (Varentsov et al., 1977). The Kamolin Member consists of ≤400 m of cross-bedded, coarse-grained sandstone and conglomerate (Klocke et al., 2017). The Childara Member consists of ≤800 m of fine- to medium-grained red sandstone, siltstone and minor conglomerate (Klocke et al., 2017). Conformably overlying the Baldshuan Formation is the Miocene Chingou Formation, which consists of regularly alternating beds of fine-grained red sandstone and conglomerate that locally exceed 2 km in aggregate thickness (Klocke et al., 2017). The Upper Miocene Tavildara Formation is composed of ≤5 km of massive, cliff-forming pebble–cobble conglomerate with rare thin beds of fine-grained red sandstone (Klocke et al., 2017; Lukens, Carrapa, Singer, & Gehrels, 2012). Unconformably overlying the Tavildara Formation are the Pliocene Karanak and Polizak Formations, which are ≤3-km thick and consist of light gray cobble–boulder conglomerate (Nikolaev, 2002).

3 | MATERIALS AND METHODS

To understand the evolution of the Tajik Basin, we measured four stratigraphic sections within the Tajik Basin: the Dashtijumb, Lattaband, Khlitoy and Shar Shar Pass sections. Sedimentological and stratigraphic data were collected from each section and include lithofacies, bedding characteristics and paleocurrent measurements. Reported paleocurrent directions (Supp. File 1) have been restored to paleo-horizontal, but do not include vertical axis rotations inferred from paleomagnetic data (Thomas et al., 1994). The Lattaband section is located near the Uzbekistan–Tajikistan border and is the section most distal to the Pamir (Figure 1b). The Lattaband section is ca. 1,450-m thick, starts in the Early Cretaceous and ends in the Paleocene to early Eocene. The Khlitoy (ca. 750-m thick) and Shar Shar Pass (ca. 250-m thick) sections are located in the central Tajik Basin (Figure 1b).

The ca. 6-km-thick Dashtijum section is most proximal to the Pamir Mountains and preserves the most complete and continuous sedimentary history of the Tajik Basin. The

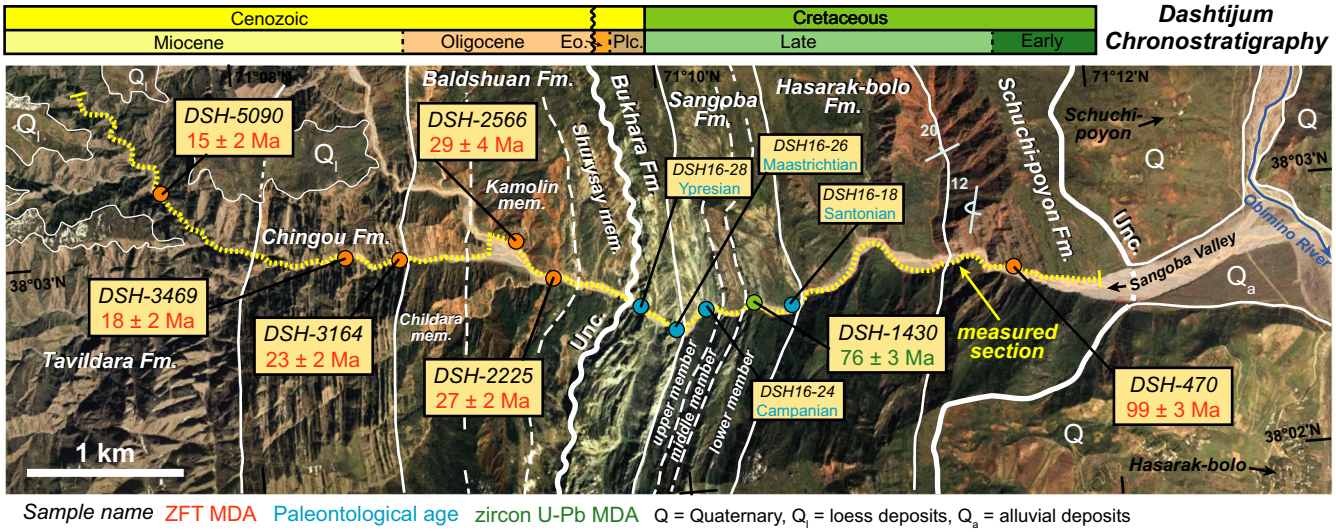

FIGURE 3 Satellite photo showing an overview of the Dashtijum measured section and locations of samples used for geochronology

section is located in the Sangoba stream valley, a tributary of the Obimino River, which is located in the Dashtijum nature reserve (Figures 1b and 3). The section starts in Lower Cretaceous strata and ends in Miocene strata. Possible type sections of three newly described stratigraphic units (Schuchi-poyon, Hasarak-bolo and Sangoba Formations) are within the Dashtijum section. The sampled sections are located along a transect-oriented orthogonal to the Pamir orogen, from the proximal foredeep (Dashtijum) to the external foreland (Lattaband). Detailed sedimentological logs (1:100 scale) of the measured sections and colour photographs with descriptions from the Dashtijum section are presented in Supplementary File 1.

Sedimentary rock samples were collected from the Dashtijum measured section for petrographic (point-counting) analysis, detrital zircon U–Pb geochronology, detrital zircon fission track (ZFT) thermochronology and micropaleontology. Details of sample preparation and methods are presented in Supplementary File 2.

4 | RESULTS

4.1 | Stratigraphic succession and sedimentary petrology

The following description of sedimentological units is based on the Dashtijum measured section (Supplementary File 1). An abbreviated summary of the main sedimentological units from the Dashtijum section is presented below. Complete sedimentological descriptions of lithofacies, interpretations of depositional environments and detailed descriptions of sandstone composition (including petrographic parameters, raw count data and recalculated modal data) are presented in Supplementary File 3.

4.1.1 | Schuchi-poyon Formation

The Schuchi-poyon Formation consists of ca. 780 m of siliciclastic strata including lenticular to tabular sandstone bodies alternating with maroon to dark red siltstone that represent fluvial channel and overbank deposits (e.g. Miall, 1996). Basal gravel conglomerate lags in trough cross-stratified sandstone channel bodies are dominated by siltstone (mainly intraclasts) and sandstone clasts. The upper part of the Schuchi-poyon Formation contains numerous thick (≤5 m), massive sandstone beds that are pervasively bioturbated and contain carbonate nodules, characteristic of paleosol development on a sandy floodplain (cf., Bown & Kraus, 1987). Sandstone from the Schuchi-poyon Formation has sublitharenite, feldspathic litharenite and litharenite compositions (Figure 4). Large percentages of lithic grains are present, including polycrystalline quartz, quartz tectonite, quartzose sandstone/quartzite fragments, volcanic fragments (mainly felsic and vitric grains), chert, shale and minor phyllite, muscovite and limestone.

4.1.2 | Hasarak-bolo Formation

The base of the Hasarak-bolo Formation is defined here by a topographic break and the abrupt appearance of predominantly fine-grained lithofacies. The unit is ca. 500-m thick and consists of siliciclastic strata including massive, maroon/green (often mottled) siltstone interbedded with widely spaced, thin (≤0.5 m) tabular, fine-grained sandstone bodies that display sedimentological evidence for deposition under tidal influence in a marginal marine setting (e.g. Dalrymple, Zaitlin, & Boyd, 1992). Desiccation cracks and evaporitic layers suggest episodic subaerial exposure and drying. Root traces, bioturbation, red-green mottling and carbonaceous

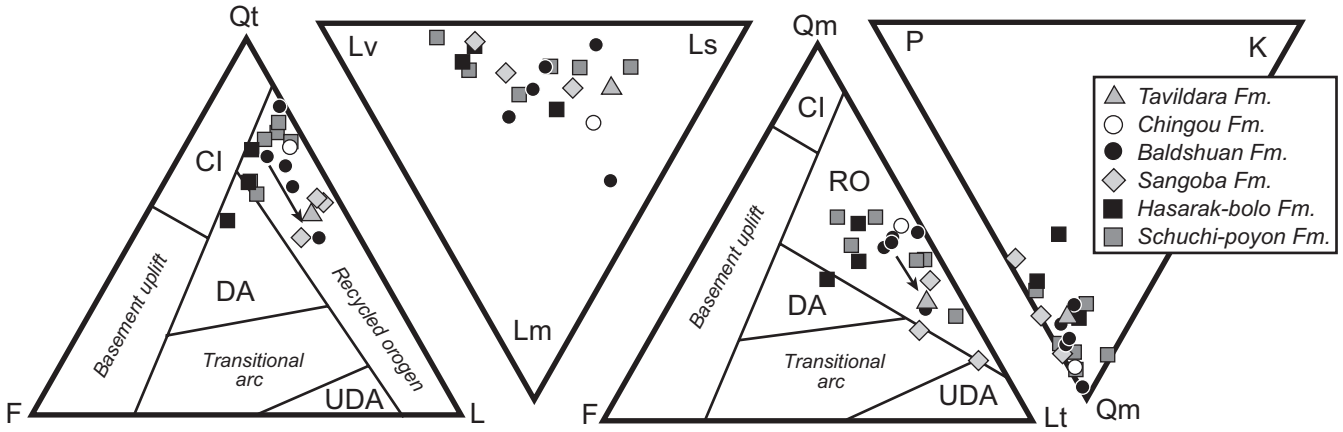

FIGURE 4 Ternary diagrams showing the composition of sandstone from the Dashtijum measured section. Qt = total quartzose grains including monocrystalline quartz (Qm) + polycrystalline quartz (Qp) + quartz tectonite (Qpt) + quartzite/sandstone (Qss) + chert + siltstone), *F* = feldspar including plagioclase (P) + orthoclase (K), L = non-quartzose lithic grains including volcanic lithic (Lv), sedimentary lithic (Ls) and metamorphic lithic (Lm) grains. Lt = total lithic grains (Ls + Lv + Lm + Qp). Compositional fields are from McBride (1963). Provenance fields are from Dickinson (1985). CI = craton interior, DA = dissected arc, UDA = undissected arc, RO = recycled orogen

debris suggest plant colonization on exposed supratidal flats (cf., Reineck & Singh, 1980). Broadly lenticular sandstone bodies with ripple cross-stratification, mud drapes, occasional trough cross-stratification and erosive bases represent tidal channels and bars (cf., Reineck & Wunderlich, 1968). Sandstone from the Hasarak-bolo Formation has feldspathic litharenite to lithic arkose compositions and contains lithic grains of similar composition and abundance to the underlying Schuchi-poyon Formation (Figure 4).

4.1.3 | Sangoba Formation

The base of the Sangoba Formation is defined by a conspicuous colour and lithologic change, from pink sandstone to dark-green laminated mudstone. and represents a major marine incursion into the Tajik–Tarim Basin (Bosboom et al., 2013, 2017). The Sangoba Formation is divided into three informal members based on lithofacies. The lower member is ca. 180-m thick and composed of dark-green, organic-rich, laminated to massive silty mudstone interbedded with thin (2–40 cm), occasionally fossiliferous, yellow-green fine- to medium-grained sandstone beds deposited in a low-gradient, mud-dominated shelf/ramp environment (e.g. Varban & Plint, 2008).

The middle member of the Sangoba formationFormation is ca. 115-m thick and is composed mostly of maroon-brown siltstone and interbedded, pink sandstone intervals, which contain a wide range of sedimentary features indicative of an overall progradational shoreface sequence ranging in paleo-water depth from the lower shoreface (cf., Hart & Plint, 1995) to a fluvial system at the top of the member (cf., Miall, 1996). Conglomerate in the upper part of the middle member is compositionally immature and contains the first granitic clasts in the Dashtijum section.

The base of the upper member of the Sangoba Formation is defined by a change from red-brown massive siltstone in the middle member to grey-green laminated mudstone and the appearance of thick (>1 m) limestone beds. Laminated mudstone and marlstone layers in the lower part of the upper member are lagoonal deposits (cf., Kendall, 1968; Wright, 1984) and contain algal laminae, coal lenses and isolated vertical burrows. The upper part of the upper member is composed chiefly of massive, fossiliferous, light green-grey mudstone interbedded with yellow-green, calcite-cemented, fine-grained sandstone characteristic of inner shelf (lower shoreface to offshore) deposition (e.g. Swift, Hudelson, Brenner, & Thompson, 1987). Sandstones from the Sangoba Formation have litharenite compositions with large percentages of volcanic lithic grains (Figure 4). The fraction of mafic volcanic fragments in sandstones from the Sangoba Formation is notably greater than it is in other sandstones in the Dashtijum measured section.

4.1.4 | Bukhara Formation

The base of the Bukhara Formation is defined by the disappearance of fine-grained calcareous sandstone beds and the appearance of thick (>1 m) fossiliferous limestone beds. The Bukhara Formation in the Dashtijum section is ca. 315-m thick and composed of limestone interbedded with siltstone, mudstone and gypsum that represent carbonate lagoon/bay to sabkha deposits (e.g. Handford, 1981). Evaporite interbedded with red siltstone is characteristic of coastal sabkhas and reflects deposition in a wadi plain to saline mud flat or salt pan environment (cf., Alsharhan & Kendall, 2003). The top of the Bukhara Formation in the Dashtijum section is covered.

4.1.5 | Baldshuan Formation

Abrupt changes in colour and lithology mark the basal contact of the Shurysay Member of the Baldshuan Formation, although in the Dashtijum section, the contact is obscured by landslides on both sides of the valley. Vlasov et al. (1991) mapped the contact between the Bukhara Formation and the Shurysay Member in the Dashtijum region as a bedding-parallel reverse fault that extends along strike for at least 50 km. However, we did not observe a discordance in the orientation of bedding across the contact, or any evidence for faulting, and identified the contact as an unconformity. This interpretation is consistent with several previous sedimentological studies in the Tajik Basin that document a regional unconformity that removes a significant part of the Eocene section (Bratash et al., 1970; Burtman, 2000; Davidzon et al., 1982; Nikolaev, 2002; Varentsov et al., 1977). The Shurysay Member principally consists of ca. 210 m of recessive orange-red siltstone with minor interbedded sandstone and conglomerate that represent shallow fluvial channel and sheet-flood deposits, consistent with the previous interpretation of Klocke et al. (2017).

The Kamolin Member is distinguished from the Shurysay Member by a greater proportion and thickness of sandstone and conglomerate beds compared to siltstone layers. Medium- to fine-grained, horizontally laminated, lenticular sandstone bodies that interfinger with, or occur as lenses within, thicker conglomerate beds and very coarse- to medium-grained, upward fining, trough cross-stratified sandstone bodies with gravel to pebble conglomerate lenses represent deposition in a gravelly braided fluvial system (e.g. Boothroyd & Ashley, 1975; Hein & Walker, 1977). Granitic clasts are common and metamorphic clasts and recycled conglomerate clasts appear for the first time at this level in the Dashtijum section.

The Childara Member of the Baldshuan Formation is generally finer-grained than the Kamolin Member and is composed primarily of stacked, fine- to medium-grained sandstone beds that fine upward to siltstone interbedded with conglomerate. The Childara Member was deposited in a mixed sandy-gravelly fluvial environment (cf., Rust, 1972; Miall, 1996). A thick zone (>300 m) of carbonate nodules, bioturbation and variegated colours associated with the redistribution of iron and magnesium compounds is indicative of superimposed calcic paleosols (Bown & Kraus, 1987; Mack, James, & Monger, 1993). Sandstones from the Baldshuan Formation have sublitharenite, feldspathic litharenite and litharenite compositions (Figure 4). The appearance of significant fractions of limestone and schistose lithic grains in the Baldshuan Formation (and higher up-section) is conspicuous.

4.1.6 | Chingou and Tavildara Formations

The base of the Chingou Formation is defined by the appearance of large pebble to cobble conglomerates that form prominent topographic ridges and cliffs. The Chingou Formation is mainly composed of gravel-bed braided river deposits (e.g. Miall, 1977; Smith, 1990) including: grey, clast-supported, well-rounded conglomerate and floodplain deposits, including interbedded orange-pink massive siltstone to very fine-grained sandstone. The alternating lithologies result in a corrugated relief pattern in outcrop. Up to cobble-size granitic clasts are conspicuous.

The Tavildara Formation is transitional with the conglomeratic upper Chingou Formation, but it can be distinguished by the disappearance of interbedded siltstone layers, an increase in maximum clast size (up to small boulder) and by less well-organized conglomerate lithofacies. Amalgamated conglomerate units in the Tavildara Formation can be over 100-m thick with limited internal erosional surfaces. Sedimentological features are consistent with deposition in a proximal braided river system associated with stream-dominated alluvial fans (e.g. Rust, 1972, 1978; DeCelles et al., 1991). The dip of bedding decreases from sub-vertical near the base of the unit to ca. 50°W near the top of the Dashtijum measured section. The measured thickness is ca. 1,600 m; however, the total thickness of the Tavildara Formation in the Dashtijum region is estimated at >3,000 m based on satellite imagery (Figure 3).

Sandstones from the Chingou and Tavildara Formations have litharenite compositions (Figure 4). Conglomerate clasts of schist and gneiss first appear in the Chingou Formation and become more abundant up-section. Most conglomerate in the Chingou and Tavildara Formations is composed of >50% granitic and carbonate clasts.

4.2 | Chronological constraints

4.2.1 | Micropaleontological data

Micropaleontological data from the Dashtijum section used for chronologic constraints is presented below. More detailed paleontological observations, photomicrographs and descriptions of key biostratigraphical markers are presented in Supplementary File 4. Sample DSH 16–18, from the base of the Sangoba Formation, contains *Watznaueria barnesiae, Micula staurophora, Lucianorhabdus cayeuxii, Eiffellithus turriseiffellii* and *Prediscosphaera cretacica*. The occurrence of *L. cayeuxii* suggests that sample DSH 16–18 is not older than Santonian. A moderately well-preserved nannofossil assemblage occurs in sample DSH 16–24, from the upper member of the Sangoba Formation, which is characterized by abundant *Watznaueria barnesae* and rare *Arkalgelskiella cymbiformis, Micula staurophora, Broinsonia* sp., *Eiffelliths*

eximius, Eiffellithus turriseiffellii, Prediscosphaera cretacica, Zeughrabdothus sp., *Staurolites ellipticus, Cretarhabdus surirellus* and *Cretarhabdus angustiforatus*. The occurrence of both *A. cymbiformis* and some specimens of *Broisonia* sp. indicate at least a Campanian age for DSH 16–24.

Two samples from the Bukhara Formation contain identifiable ostracod assemblages. Sample DSH 16–26 (lower Bukhara Formation) is characterized by abundant rudist remains, echinoids, corals, bivalves, some ostracods and large benthic foraminifera, tentatively assigned to the genera *Omphalocyclus* and *Lafitteina*. The occurrences of these two foraminiferal genera indicate a Maastrichtian age for sample DSH 16–26. The most common identified taxa in sample DSH 16–28 (upper Bukhara Formation) are *Echinocythereis isabenana* Oertli, *Paracypris troslien-sis* Apostolescu, *Paracyprideis similis* Triebel, *Krithe* sp. aff *K. rutoti* Keij, *Cytherella compressa* (von Münster), *Eocytheropteron sherborni* Bowen, with rare, poorly preserved specimens of *Xestoleberis subglobosa* (Bosquet), *Loxoconcha* sp. and *Paracytheretta* sp.. This ostracod assemblage is assigned to the 6c (*Echinocythereis reticulatissima*) and 7 (*Novocypris whitecliffensis*) Paleogene ostracod zones (Keen, 1978), indicative of the Lower Eocene (Ypresian), equivalent to the NP 11–13 calcareous nannofossil zones and P6–P9 planktonic foraminiferal zones (ca. 54–47 Ma).

4.2.2 | Geochronological and thermochronological data

Seven sandstone samples from the Dashtijum section were analysed for detrital zircon U–Pb geochronology. Sample DSH-470 was collected from the Schuchi-poyon Formation and has a minimum detrital age population of 221 ± 5 Ma, defined by three zircon grains (Figure 5a). Sample DSH-1430 was collected from the lower member of the Sangoba Formation and has a minimum age population of 76 ± 3 Ma, defined by three zircon grains (Figure 5a). Samples DSH-2225 and DSH-2566 (Kamolin Member of the Baldshuan Formation), DSH-3164 (Chingou Formation) and DSH-3469 (Tavildara Formation) all have minimum detrital zircon U–Pb age populations of ca. 44–43 Ma, defined by 4–52 grains (Figure 5a). Sample DSH-5090 was collected from the Tavildara Formation and has a minimum age population of 35 ± 2 Ma, defined by 30 zircon grains. Sample DSH-5090 is the only sample from the Dashtijum section with a well-defined (8 grains) mid-Cretaceous zircon U–Pb age population (101 ± 4 Ma). All Dashtijum samples except DSH-2225 and DSH-2566 have prominent ca. 200–300 Ma age populations.

Two samples from the Lattaband section were analysed for detrital zircon U–Pb geochronology (Figure 5a). The minimum age population for sample LAT-01 is 242 ± 4 Ma, defined by 11 grains and the minimum age population for sample LAT-1022 is 213 ± 5 Ma, defined by 3 grains. Both samples also have prominent age populations of ca. 300 Ma and ca. 400 Ma. Based on previous geologic mapping (Vlasov et al., 1991), the depositional age for sample LAT-01 is estimated to be Upper Cretaceous and the depositional age of sample LAT-1022 is estimated to be Paleocene. Complete zircon U–Pb data for the Dashtijum and Lattband section samples are presented in Supplementary Table 1.

Six sandstone samples from the Dashtijum section were analysed for detrital ZFT thermochronology (Figure 5b). Sample DSH-470 from the Schuchi-poyon Formation has a single large detrital ZFT age population of 99 ± 6 Ma. Sample DSH-2225 from the Kamolin Member of the Baldshuan Formation has a young age population of 27 ± 2 Ma and an older age population of 93 ± 8 Ma. Sample DSH-2566, also from the Kamolin Member of the Baldshuan Formation, has a young age population of 29 ± 4 Ma and an older age population of 106 ± 8 Ma. Sample DSH-3164 from the Chingou Formation has a young detrital ZFT age population of 23 ± 2 Ma and older age population of 98 ± 6 Ma. Sample DSH-3469 from the Tavildara Formation has a young age population of 18 ± 2 Ma and older age population of 92 ± 6 Ma. Sample DSH-5090 from the Tavildara Formation has a young age population of 15 ± 2 Ma and an older age population of 88 ± 8 Ma. Double dating shows that the middle to Late Cretaceous ZFT ages from sample DSH-5090 were obtained from two zircon U–Pb age populations. The first population has mid-Cretaceous (110–100 Ma) zircon U–Pb ages and the second population has Early Mesozoic to Paleozoic zircon U–Pb ages. Complete ZFT data are presented in Supplementary Table 2.

5 | DISCUSSION

5.1 | Age calibration and stratigraphic correlations

Strata equivalent with the Schuchi-poyon Formation in the Dashtijum region were mapped as Early Cretaceous by Vlasov, Pyzhjanov, and Loziev (1964). This age assignment agrees well with detrital ZFT data from the Schuchi-poyon Formation, which are characterized by a single mid-Cretaceous age population (99 ± 6 Ma; Figure 5b) that is interpreted as the maximum depositional age of the unit. The youngest detrital zircon U–Pb age population from the Schuchi-poyon Formation (ca. 220 Ma) is significantly older and is not interpreted to reflect depositional age (Figure 5a). Strata equivalent with the Hasarak-bolo Formation were mapped as Late Cretaceous by Vlasov et al. (1964). Fine-grained samples collected from the Hasarak-bolo Formation for micropaleontological analysis were barren.

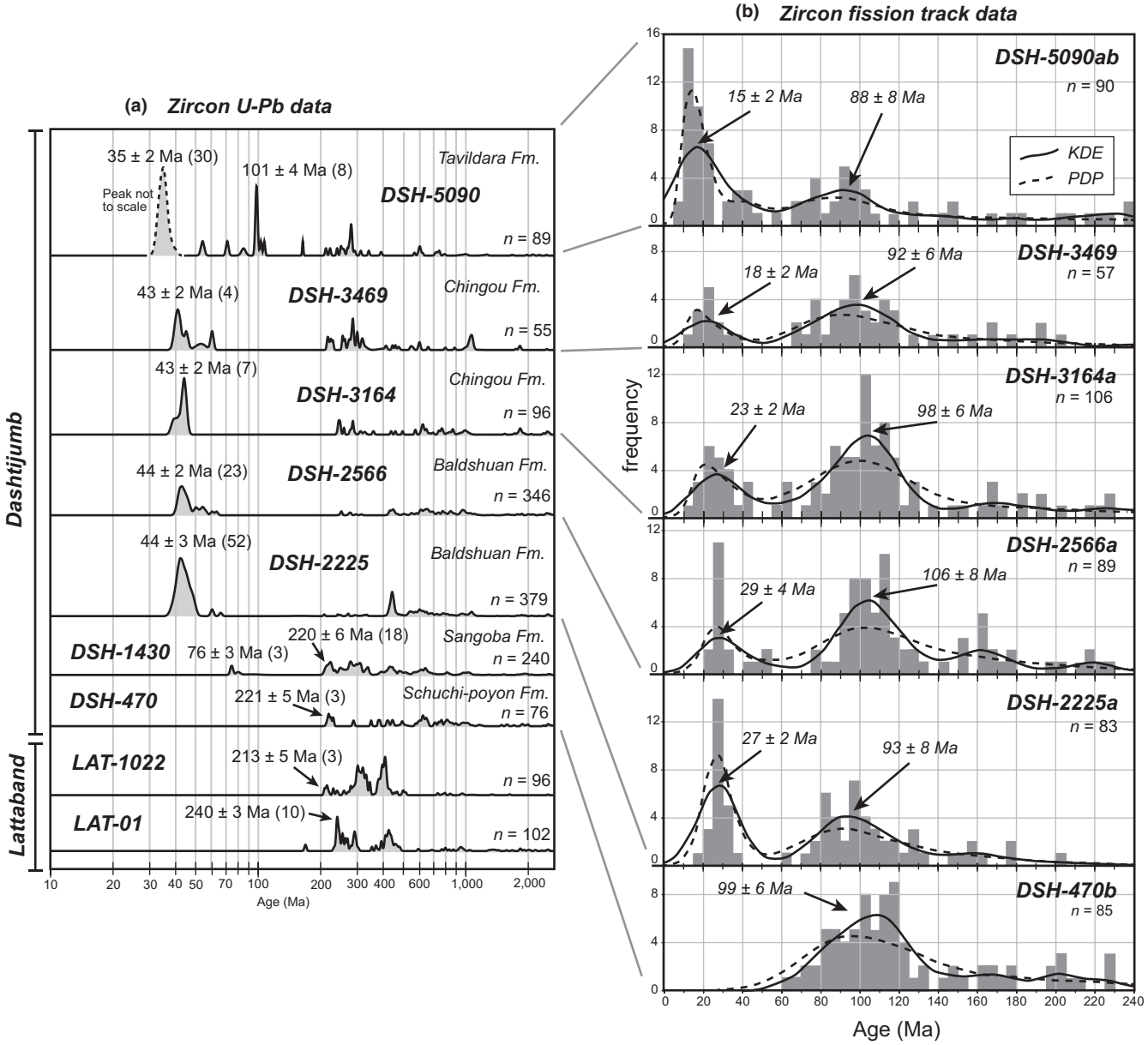

FIGURE 5 (a) Detrital zircon U–Pb data from sandstone in the Dashtijum measured section shown as normalized probability density diagrams. Numbers in parentheses are the number of grains/analyses used to calculated weighted mean age for an age population/peak. (b) Detrital zircon fission track (ZFT) data for select samples presented in a. Grey vertical bars are histograms for individual ZFT ages. Solid curves are kernel density estimates (KDE) of ages, dashed curves are probability density plots (PDP) of ages. Labelled age populations are based on KDE curves

Micropaleontological data indicate that the lower member of the Sangoba Formation is not older than Santonian (< ca. 86 Ma) and that the upper member of the Sangoba Formation is Campanian (> ca. 70 Ma). These age assignments are consistent with the youngest detrital zircon U–Pb age population (76 ± 3 Ma) collected from the lower member of the Sangoba Formation, which is interpreted as the maximum depositional age (Figure 5a). Micropaleontological data from the lower Bukhara Formation suggest a Maastrichtian to early Paleocene age and data from the upper Bukhara Formation indicate an Ypresian age (ca. 54–47 Ma). These age estimates are consistent with regional age assignments of the Bukhara Formation throughout the Tajik Basin (Davidzon et al., 1982).

Detrital zircon U–Pb age data from the Baldshuan, Chingou and Tavildara Formations all display prominent Eocene age populations, which are the youngest populations in each sample and young up-section (Figure 5a). However, these ages are not interpreted to reflect depositional age, but rather to represent a provenance and exhumation signature The Eocene detrital zircon U–Pb age populations are consistent with the age of the Vanj magmatic complex in the Central Pamir terrane (45–35 Ma; Figure 1a; Chapman, Scoggin, et al., 2018), which is a major magmatic event in the Pamir and

dominates zircon U–Pb age populations of modern river sand samples (Carrapa et al., 2014; Lukens et al., 2012). Younger potential sources of zircon are present in the Pamir, chiefly ca. 10–20 Ma leucogranite bodies associated with the Pamir gneiss domes and the ca. 11 Ma potassic Taxkorgan complex (Chapman, Scoggin, et al., 2018; Jiang et al., 2012; Stearns, Hacker, Ratschbacher, Rutte, & Kylander-Clark, 2015), but zircon with U–Pb ages younger than ca. 35 Ma was not encountered in the Tajik Basin sandstone samples.

The youngest detrital ZFT age populations from samples of the Baldshuan (29 ± 4 Ma and 27 ± 2 Ma), Chingou (23 ± 2 Ma and 18 ± 2 Ma) and Tavildara (15 ± 2 Ma) Formations are interpreted to represent the maximum depositional ages for each unit. The youngest age populations in each sample generally become younger up-section (Figure 5b) and double-dating (U–Pb + ZFT) shows that grains with young ZFT ages have a wide range of zircon U–Pb ages (Paleozoic to Eocene; Supplementary Table 2), which suggests that the detrital ZFT cooling ages are related to exhumation, rather than due to thermal overprinting. The proposed ages for the Baldshuan Formation and younger units are consistent with previous age estimates (Klocke et al., 2017; Nikolaev, 2002), although these coarse-grained units remain relatively poorly dated. The sample from the Tavildara Formation was collected near the base of the unit and there is no age constraint for the remainder of the unit.

Geochronologic data from the Dashtijum section suggests that the disconformity between the Bukhara Formation and the Baldshuan Formation is middle Eocene to lower Oligocene (ca. 30–50 Ma; Figure 2). Accounting for age ranges and data uncertainty, the disconformity could be as old as ca. 54 Ma and as young as ca. 25 Ma, with the caveat that the minimum age is constrained by maximum depositional ages, not an absolute age.

5.2 | Subsidence history

Subsidence analysis (Van Hinte, 1978) was performed on the Dastijum measured section based on the sedimentological, geochronological and paleontological results presented above (Figure 6). Input data and results are reported in Supplementary Table 3. The total thickness of the Lower Cretaceous section was adopted from Vlasov et al. (1964). Eustatic changes in sea level were not included. Original porosity and compaction coefficients for different rock types were adopted from Sclater and Christie (1980) for sediment decompaction. Tectonic subsidence was calculated by local isostatic backstripping (Steckler & Watts, 1978). For comparison, tectonic subsidence from this study is plotted with Leith's (1985) mean tectonic subsidence curve for the Tajik Basin (Figure 6).

Tectonic subsidence was slow (ca. 0.01 mm/yr) during the Early Cretaceous. Accelerated subsidence (up to ca. 0.04 mm/yr) during the mid-Cretaceous coincided with deposition of the Schuchi-poyon Formation. From mid-Cretaceous to Eocene, tectonic subsidence declined exponentially, resulting

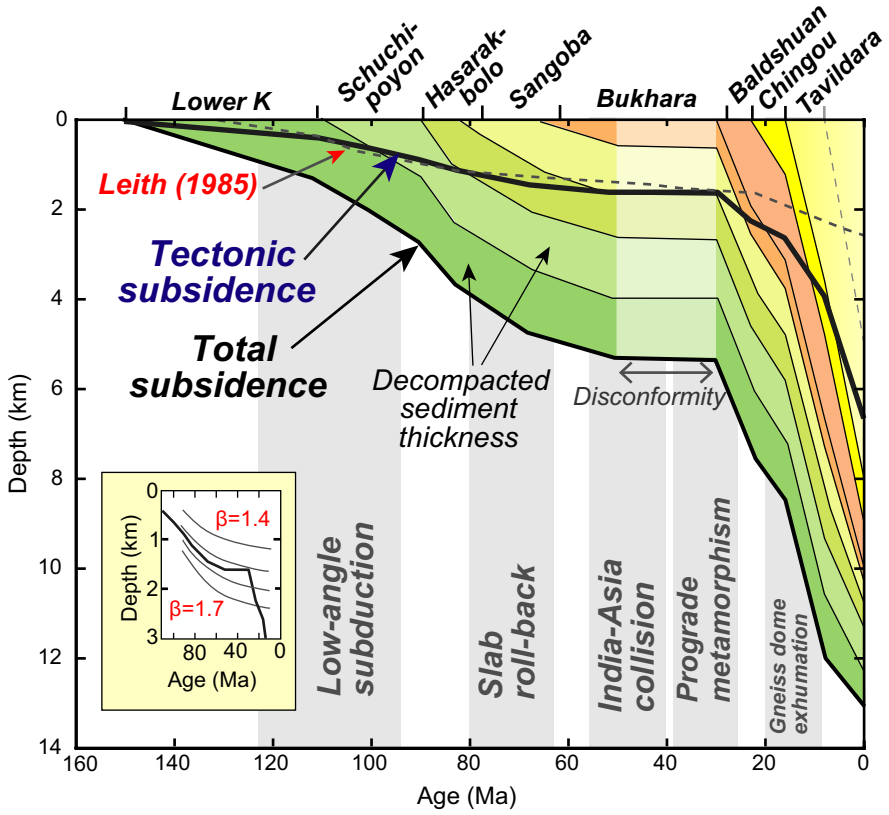

FIGURE 6 Subsidence analysis of the Dashtijum measured section including total subsidence (black curve) and tectonic subsidence (blue curve), which is compared to the tectonics subsidence of Leith (1985; red curve). The inset plot shows a portion of the tectonic subsidence curve with subsidence (red lines) predicted by a uniform stretching model for different stretch factors (β). Regional tectonic events are shown in grey bars

in a concave-up subsidence curve (Figure 6). Subsidence rates were very slow (<0.01 mm/yr) during the middle-to-late Eocene, although the slow rates may be exaggerated if there is significant missing section above the Bukhara Formation. Starting with deposition of the Baldshuan Formation, tectonic subsidence abruptly increased (>0.1 mm/yr). Tectonic subsidence continued to accelerate during the Oligocene and Miocene (>0.3 mm/yr), resulting in a concave-down subsidence curve.

To further explore regional subsidence patterns, measured sections from this study and from previous studies were correlated for Cretaceous (Figure 7) and Cenozoic (Figure 8) strata and then projected onto a cross section-oriented ca. E–W across the Tajik Basin. The spacing of the measured sections in Figure 7 has been restored to account for shortening in the Tajik thrust belt using the structural reconstruction in Chapman et al. (2017). From west to east (towards the Pamir Mountains) the Cretaceous section thickens from ca. 1 km in the Tian Shan to almost 3 km in the Dastijum region.

5.3 | Sediment provenance

Traditionally, the Tajik Basin has been divided into a lower Oligocene and older pre-tectonic succession and an upper Oligocene to Pliocene synorogenic succession related to the uplift of the Pamir Mountains and, to a lesser extent, the Tian Shan (Burtman & Molnar, 1993; Klocke et al., 2017; Leith, 1982, 1985; Nikolaev, 2002; Varentsov et al., 1977). Recently, Carrapa et al. (2014) proposed extending the initiation of synorogenic sedimentation back in time, to at least the Eocene. Results of this study suggest that the Pamir has been the primary source of sediment to the Tajik Basin since the Cretaceous.

5.3.1 | Cretaceous strata

The youngest detrital zircon U–Pb age populations (ca. 220 Ma) in the lower to middle Cretaceous Schuchi-poyon Formation and Upper Cretaceous Sangoba Formation in the Dashtijum

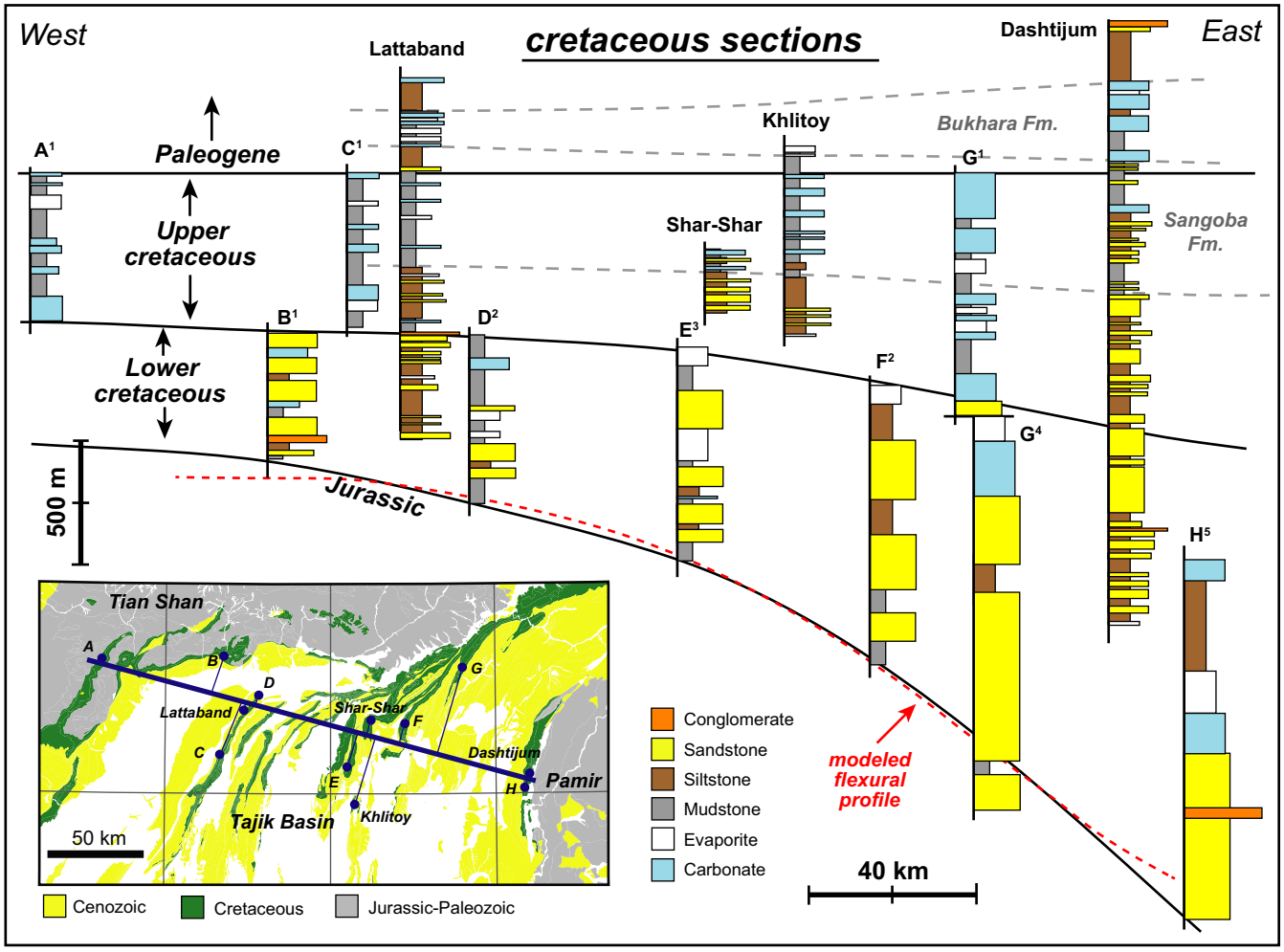

FIGURE 7 Diagram of Cretaceous and lower Paleogene stratigraphic columns from measured sections projected on a cross section (inset map, thick blue line) and flattened on the Cretaceous–Paleogene boundary. Stratigraphic columns labelled with letters (A–H) are previously published (1 = Djalilov, 1971; 2 = Simakov, 1952; 3 = Filonov & Koroly, 1966; 4 = Muftiev & Shachnev, 1967; 5 = Vlasov et al., 1964). The red-dashed line is based on flexural modelling of an unbroken plate with a flexural rigidity of 1 × 1,023 Nm

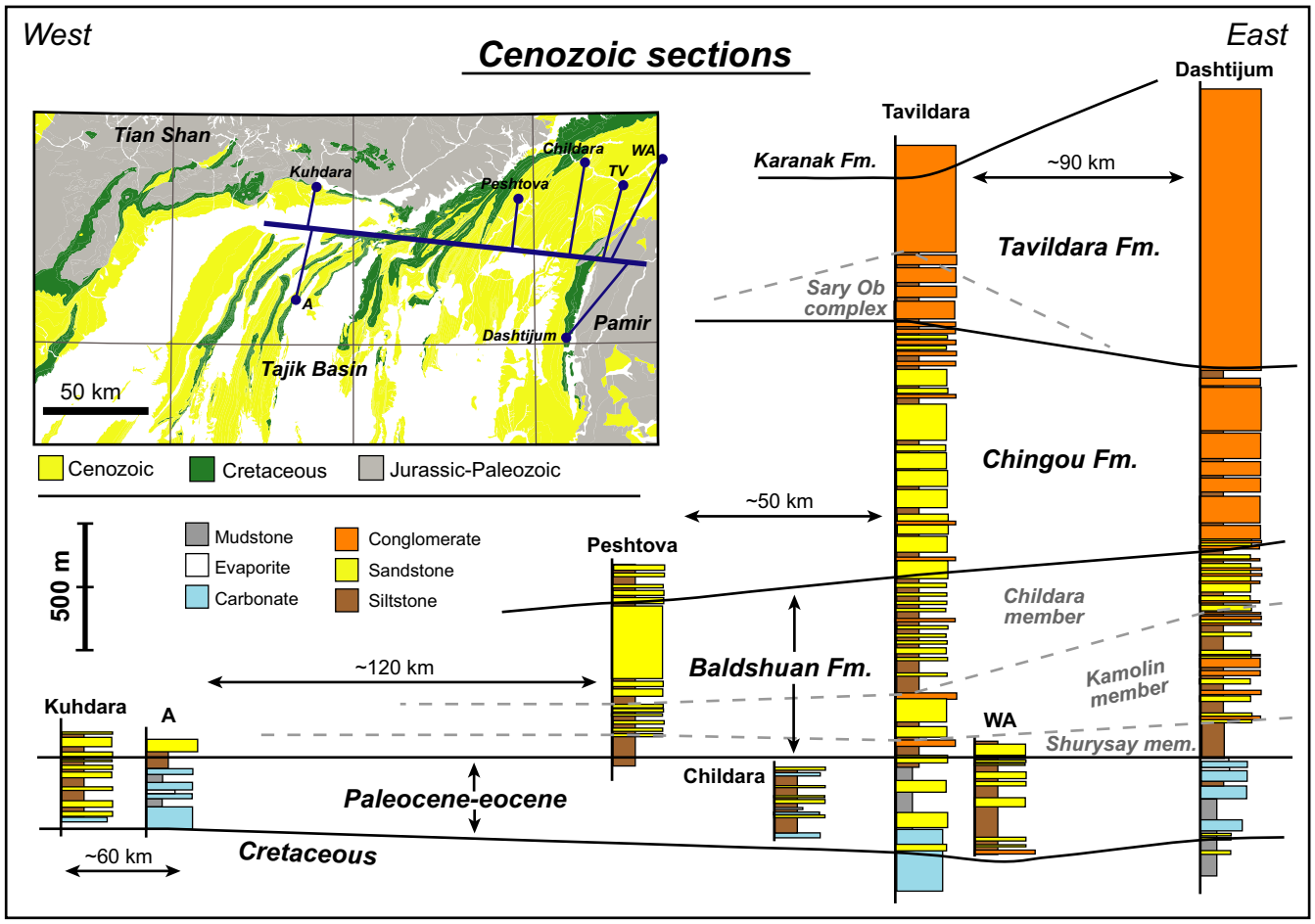

FIGURE 8 Diagram of Cenozoic stratigraphic columns from measured sections projected on a cross section (inset map, thick blue line) and flattened on the Eocene-Oligocene boundary. Previously published stratigraphic columns are: A (Davidzon et al., 1982), Kuhdara and Childara (Bosboom et al., 2017), Tavildara (TV) (Klocke et al., 2017) and Peshtova and WA (Carrapa et al., 2015). The WA and Dashtijum sections are projected onto the section at an angle to represent their relative distance from the Pamir Mountain front

section (Figure 5a) are consistent with the age of intrusive and metavolcaniclastic rocks in the Karakul–Mazar subduction–accretion complex in the north Pamir (Robinson et al., 2012; Schmalholz, 2004). No significant exposures of magmatic rocks younger than ca. 250 Ma exist in the westernmost Tian Shan (Käßner et al., 2016; Worthington et al., 2017). Older, Paleozoic zircon U–Pb age populations could have been derived from either the Tian Shan or the Pamir Mountains. Paleogeographic reconstructions suggest that the westernmost Tian Shan was partly to completely covered by sedimentary rocks from the Cretaceous to Miocene (Burtman, 2000; Carrapa et al., 2014; De Pelsmaeker et al., 2018), which suggests that the Pamir was the primary sedimentary source during the Cretaceous. Although sediment previously eroded from the Tian Shan could have been recycled into the Tajik Basin during the Cretaceous, sandstones from the Cretaceous Schuchi-poyon, Hasarak-bolo and Sangoba Formations in the Dashtijum section are compositionally immature (litharenite) and have mineral assemblages (e.g. mica) suggesting limited sediment transport and recycling, also favoring the Pamir as a primary sediment source.

All of the samples analysed from the Tajik Basin, regardless of depositional age, display a prominent mid-Cretaceous detrital ZFT age population. These ages generally fall between 106 Ma and 90 Ma (Figure 5b). A few analyses from sample DSH-5090 could be related to magmatic cooling, however double-dating indicates that the majority of mid-Cretaceous ZFT ages in sample DSH-5090 and all of the mid-Cretaceous ZFT ages in the other samples are exhumation ages. We interpret the mid-Cretaceous detrital ZFT age populations in the Tajik Basin samples to be derived from the Karakul–Mazar complex. Schmalholz (2004) reported Cretaceous bedrock ZFT ages (122–108 Ma) from the Karakul–Mazar complex and there is a regionally extensive mid-Cretaceous (ca. 100 Ma) exhumation event associated with crustal shortening in the Karakul–Mazar complex (Robinson et al., 2004, 2007, 2012). Because the Pamir is the predominant source of sediment for upper Oligocene to Pliocene units (Klocke et al., 2017), we deduce that the mid-Cretaceous ZFT age population was also derived from the Pamir prior to the Oligocene and during the Cretaceous. The relatively large fraction

(10%–15% of total grains) of volcanic lithic fragments in sandstone from Cretaceous strata in the Dashtijum section is consistent with derivation from a magmatic arc.

Cretaceous detrital zircon U–Pb age populations first appear in the Upper Cretaceous Sangoba Formation. The zircon U–Pb age population (76 ± 3 Ma) in the Sangoba Formation is consistent with the age (80–70 Ma) of relatively mafic igneous rocks exposed in the Central Pamir terrane that have been associated with regional extension related to Neotethyan slab rollback (Chapman, Scoggin, et al., 2018; Schwab et al., 2004). Sandstone from the Sangoba Formation has the highest percentage of mafic volcanic lithic fragments (ca. 20% of volcanic lithic grains) compared to all other units studied in the basin. Granitic clasts (chiefly potassium feldspar-rich alkali granitoids) and marine limestone clasts first appear in Sangoba Formation conglomerate in the Dashtijum section. These clasts are interpreted to have originated in the Kunlun arc and Permian section in the north Pamir Mountains.

In summary, sandstone composition, zircon U–Pb crystallization ages and ZFT exhumation ages all suggest that the Cretaceous units in the Tajik Basin (Schuchi-poyon, Hasarak-bolo and Sangoba Formations) were primarily derived from the northern Pamir, including the Karakul–Mazar complex. Compositional changes in the Sangoba Formation suggest that the Central Pamir terrane started supplying sediment to the Tajik Basin during the Late Cretaceous.

5.3.2 | Cenozoic strata

The prominent Eocene zircon U–Pb age population in the Baldshuan, Chingou and Tavildara Formations (Figure 5a) in the Dashtijum section is consistent with the age of the Vanj magmatic complex (ca. 45–35 Ma) in the Central Pamir terrane (Chapman, Scoggin, et al., 2018). Regionally, no other Eocene igneous rocks are exposed that could have supplied zircon to the Tajik Basin. These results suggest that the Central Pamir terrane was a significant sediment source by the Oligocene. Prominent Triassic zircon U–Pb age populations in Cretaceous units in the Dashtijum section are minor or absent in the Cenozoic formations.

The up-section increase in metamorphic lithic fragments in sandstones from the Baldshuan Formation (Oligocene–lower Miocene) and appearance of metamorphic conglomerate clasts in the Chingou Formation (mid-Miocene) and younger deposits in the Dashtijum section is consistent with an unroofing sequence that exhumed the Pamir gneiss domes. The up-section increases in carbonate sedimentary lithic grains in sandstone and carbonate clasts in conglomerate in the Oligocene and younger section are interpreted to indicate increasing supply of detritus from the Permian carbonate succession exposed in the northern Pamir (Burtman & Molnar, 1993). Carbonate rocks are also common in the South Pamir terrane, but widespread cobble-sized carbonate clasts in Miocene conglomerate from the Dashtijum section suggest limited transport distances.

The Tavildara Formation in the Dashtijum section contains a prominent ca. 101 Ma zircon U–Pb age population, which is not present in older strata (Figure 5a). This age population is similar to the age of the South Pamir batholith in the South Pamir terrane (Chapman, Scoggin, et al., 2018). This batholith is volumetrically the most significant igneous body in the Pamir (Schwab et al., 2004) and detrital zircons from modern rivers draining the South Pamir terrane have large mid-Cretaceous U–Pb age populations (Carrapa et al., 2014; Lukens et al., 2012). The data suggest that Late Miocene drainage networks extended into the South Pamir terrane.

5.4 | Basin forming mechanisms

5.4.1 | The lower to mid-cretaceous Tajik Basin

Based on observations and data summarized below, the Lower to mid-Cretaceous Tajik Basin is interpreted as a retroarc foreland basin associated with growth of the Pamir and northward subduction of Tethyan oceanic lithosphere (Figure 9). During the Early to mid-Cretaceous, low-angle subduction has been proposed to have caused the northward migration of continental arc magmatism into the South Pamir terrane (Chapman, Scoggin, et al., 2018) and widespread shortening and crustal thickening within the Pamir (Chapman, Robinson, et al., 2018; Robinson, 2015). This episode of crustal thickening may have produced a flexural basin in the Pamir foreland and supplied sediment to that basin. Sandstone compositions from the lower to mid-Cretaceous Schuchi-poyon Formation indicate a recycled orogen provenance (Figure 4). Specifically, compositional, geochronologic and thermochronologic data all connect the Schuchi-poyon Formation deposits to the Karakul–Mazar complex in the northern Pamir. A foreland basin containing detritus derived from the Karakul–Mazar complex is consistent with previous studies that documented mid-Cretaceous shortening and exhumation in the Karakul–Mazar complex (Robinson et al., 2004, 2007).

The subsidence pattern for Lower to mid-Cretaceous strata in the Dashtijum section is convex-up, consistent with foreland basin subsidence patterns (Xie & Heller, 2009), although the concavity inflection between the Lower and Upper Cretaceous section is not well defined (Figure 6). Lower to mid-Cretaceous rocks in the Tajik Basin thicken towards the Pamir (Figure 7), also characteristic of foreland basin sedimentation (Beaumont, 1981). The wavelength (basin half width = ca. 200 km) and geometry (exponential increase in sediment thickness towards the Pamir mountain front) of the Lower to mid-Cretaceous Tajik Basin is typical for a foredeep generated by elastic flexure (DeCelles, 2012). A flexural profile for bending of a continuous (unbroken) plate was modeled (2D flexure equation;

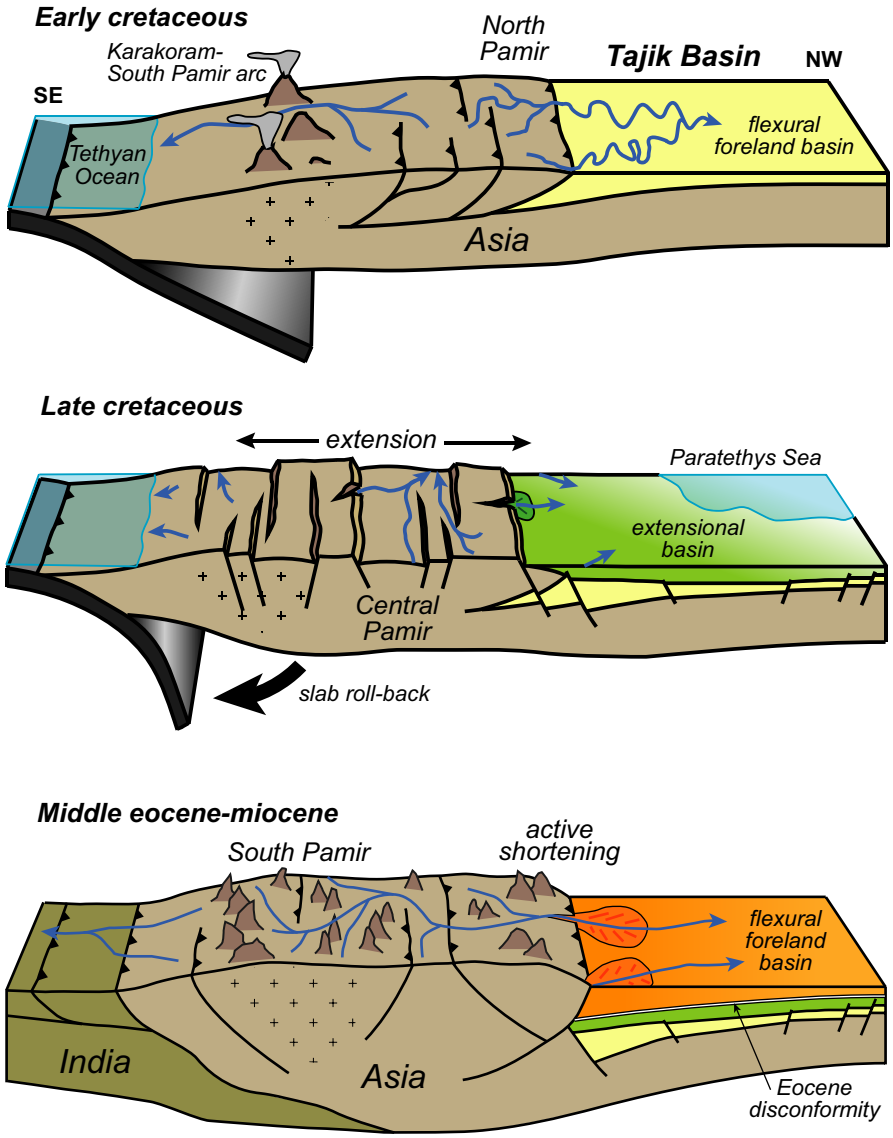

FIGURE 9 Schematic cross sections showing the proposed development of the Tajik Basin. During the Early Cretaceous, northward subduction of Tehtyan oceanic lithosphere built the Karakoram–South Pamir arc and caused crustal thickening in the Pamir. This thickening produced a retroarc flexural foreland basin during the Early Cretaceous. Slab rollback during the Late Cretaceous may have caused regional extension followed by slow thermal subsidence in the Tajik Basin. Contemporaneous with India–Asia collision, a flexural forebulge passed through the Tajik Basin and caused a ca. 50–30 Ma regional disconformity. The disconformity marks the base of the Cenozoic foreland basin sequence. Oligocene and younger rocks were deposited in a foredeep depozone

centered finite-difference method; e.g. Chapman et al., 2017) to approximate the shape of the Cretaceous basin (red dashed line, Figure 7). The parameters used were 2,500 kg/m^3 basin fill density, 640 m high and 300 km long rectangular load with 2,700 kg/m^3 density and 25 km effective elastic thickness (ca. 1 × 1,023 Nm flexural rigidity), which is comparable to the upper-end of modern estimates for effective elastic thickness (15–25 km) based on gravity data (McNutt, Diament, & Kogan, 1988; Wang, Feng, & Hsu, 1997) and flexure of the modern Tajik Basin (Chapman et al., 2017). Upper Cretaceous (e.g. Sangoba Formation; Figure 7) sediment thickness in the Tajik Basin is more uniform and does not exhibit marked thickening towards the Pamir.

5.4.2 | The Upper Cretaceous–Lower Paleogene Tajik Basin

The Upper Cretaceous to early Paleogene Tajik Basin (Hasarak-bolo Formation to Bukhara Formation) is tentatively interpreted as an extensional basin associated with lithospheric stretching (Figure 9) based on the observations and data discussed below. The Hasarak-bolo and Bukhara Formations define a multi-kilometre-thick, upward-fining succession characterized by rising relative sea-level and a decrease in tectonic subsidence rate (Figure 6). Concave up subsidence patterns are a standard indicator of extensional/rift basins and can be modeled with a simple uniform stretching model (McKenzie, 1978). Modeled subsidence is compared to the Dashtijum tectonic subsidence curve in the inset in Figure 6 for a range of stretch factors (β), using a crustal thickness/lithospheric thickness ratio (γ_c/γ_L) of 0.3. Upper Cretaceous subsidence is consistent with a stretch factor of 1.5 to 1.6. The upper Bukhara Formation also contains a regionally extensive carbonate sequence that extends across the entire Tajik Basin (Bosboom et al., 2017; Burtman, 2000), which we propose may be a classic "steer's head" sequence related to thermal decay and relative sea-level rise following lithospheric extension (Dewey, 1982; White & McKenzie,

1988). A Late Paleocene to Early Eocene transgression documented in the Tarim Basin (lower member of the Qimugen Formation) overlaps in age with the Bukhara Formation in the Tajik Basin and may be genetically related (Bosboom et al., 2017). However, Kaya et al. (2019) suggested that the transgression associated with the Qimugen Formation in the Tarim Basin is related to eustatic forcing. Regional thickness patterns indicate that Upper Cretaceous to early Paleogene subsidence was broadly uniform (Figure 7) and Burtman (2000) reported that the Upper Cretaceous to early Paleogene section thickens slightly towards the middle of the Tajik Basin, which may also be consistent with an extensional (rather than flexural) basin.

Sandstone petrographic data from Upper Cretaceous to lower Paleogene rocks in the Dashtijum section are difficult to interpret. Sandstone compositions from all Cretaceous units plot in recycled orogenic fields on both Qt/F/L and Qm/F/Lt ternary diagrams (Figure 4), normally characteristic of foreland basin deposits (Dickinson, 1985; Garzanti, Doglioni, Vezzoli, & Ando, 2007). However, continental rifts are not explicitly included on tectonic-provenance discrimination plots because of the great diversity of potential source rocks (Ingersoll, 1990). Cretaceous sandstones from the Tajik Basin are immature and contain high percentages of sedimentary and volcanic lithic fragments, typical of sand derived by shallow exhumation and erosion of upper crustal volcanic and sedimentary cover sequences (Garzanti et al., 2007). These sandstone compositions could be produced by erosion of a thrust belt or by erosion of uplifted rift flanks.

During the Late Cretaceous, rollback of the Tethyan slab and foundering of previously subducted oceanic lithosphere caused localized hinterland extension and extension-related magmatism in the Central Pamir terrane, Karakoram terrane and within the Kohistan arc (Figure 9) (e.g. Debon & Ali-Khan, 1996; Burg, 2011; Chapman, Scoggin, et al., 2018). Late Cretaceous mafic igneous rocks in the westernmost Tian Shan have been associated with a small plume or extension (Käßner et al., 2016; Simonov, Mikolaichuk, Safonova, Kotlyarov, & Kovyazin, 2015; Sobel & Arnaud, 2000). The relative abundance of mafic volcanic lithic fragments in the Sangoba Formation and provenance data linking the Sangoba Formation to mafic, extension related, igneous rocks in the Central Pamir terrane supports the interpretation that the Upper Cretaceous to early Paleogene Tajik Basin is extension related.

The main weakness of our interpretation of the upper Cretaceous to lower Paleogene section as part of an extensional basin is that there are no documented normal faults of the correct age in the Tajik Basin (cf., Hamburger et al., 1992). If present, these structures may be obscured by the Tajik fold–thrust belt (Chapman et al., 2017) or covered by younger sediments. Another possibility is that the region was dominated by thermal subsidence.

5.4.3 | The Upper Paleogene – Miocene Tajik Basin

Above the middle Eocene to lower Oligocene disconformity in the Dashtijum section, subsidence and sediment accumulation rates increase (Figure 6), grain size increases up-section, sandstone compositions indicate a recycled orogenic provenance and conglomerate compositions indicate an overall unroofing trend. Based on these observations, we interpret the middle to lower Eocene section to represent deposition in the foredeep depozone of a foreland basin system (e.g. DeCelles & Giles, 1996), which supports previous interpretations of the Cenozoic Tajik Basin as a foreland basin (Burtman, 2000; Burtman & Molnar, 1993; Carrapa et al., 2015; Klocke et al., 2017; Nikolaev, 2002). The Eocene disconformity (ca. 50–30 Ma) in the Dashtijum section is not a local feature; similar disconformities and weak angular unconformities cut out upper Eocene rocks throughout the Tajik Basin (Bratash et al., 1970; Burtman, 2000; Davidzon et al., 1982; Djalilov, 1971; Nikolaev, 2002). A prolonged (>10 Myr) period of low sediment accumulation or erosion that precedes rapid foredeep sediment accumulation is commonly interpreted to mark the passage of a flexural forebulge (e.g. Crampton & Allen, 1995; DeCelles, Kapp, Gehrels, & Ding, 2014; Sinclair, Coakley, Allen, & Watts, 1991). The presence of a forebulge in the middle Eocene supports the hypothesis that the Tajik Basin was part of a foreland basin since at last ca. 45 Ma (Carrapa et al., 2015). The onset of rapid subsidence in the southwest Tarim Basin is dated at 41 Ma (Blayney et al., 2019). Assuming a flexural rigidity of $5 \times 1{,}022$ Nm for the Cenozoic Tajik Basin lithosphere (Chapman et al., 2017) and a 20 Myr depositional hiatus (ca. 30–50 Ma), the forebulge was ca. 220 km wide and migrated at a rate of ca. 11 mm/yr, which is the sum of the shortening rate and thrust belt propagation rate (DeCelles & DeCelles, 2001). Based on cross section reconstructions and thermokinematic modeling, Chapman et al. (2017) suggested that the Neogene to modern shortening rate in the Tajik thrust belt is 4–8 mm/yr.

The Eocene age of the Dashtijum disconformity is slightly younger than estimates for the onset of India–Asia collision in the western Himalaya (ca. 55 Ma; Ding et al., 2016; Najman et al., 2017) and overlaps with the onset of prograde metamorphism in the Pamir (45–30 Ma; Smit, Ratschbacher, Kooijman, & Stearns, 2014; Stearns et al., 2015; Hacker et al., 2017). The Cenozoic Tajik Basin is interpreted as a retrowedge foreland basin system (e.g. Naylor & Sinclair, 2008) that formed on Asian continental lithosphere in response to India–Asia collision to the south (Figure 9). Although exhumation of the Pamir gneiss domes during the Miocene has been linked to a regional extensional event (Hacker et al., 2017), subsidence in the Tajik Basin continued to accelerate during this time.

5.5 | The Pamir Foreland Basin System

An unresolved question is whether or not the depositional and tectonic history of the Tajik Basin, presently located west of the Pamir, is applicable to the Mesozoic–Cenozoic Pamir foreland basin system as a whole, which also includes the westernmost Tarim Basin, presently located east of the Pamir, and remnants (e.g. Alai Valley; Figure 1) of a basin system that was located north of the Pamir (hereafter called the Alai Basin). Paleomagnetic studies in the Tajik Basin suggest up to ca 50° counterclockwise vertical rotations since the Eocene (Thomas et al., 1994) and have been used to support models of radial thrusting and rotation of the northwest Pamir margin to create the Pamir salient (Bourgeois, Cobbold, Rouby, Thomas, & Shein, 1997; Burtman & Molnar, 1993; Cowgill, 2010; Liu et al., 2017; Sobel et al., 2013). In this scenario, the Mesozoic to early Paleogene Tajik Basin may have had an orientation analogous to the Alai Basin in the past. Conversely, limited amounts (< 50 km) of Cenozoic shortening (Chapman et al., 2017; Coutand et al., 2002; Li, Chen, Thompson, Burbank, & Xiao, 2012) and limited (<60 km) sediment transport distances during the Cenozoic (Chen et al., 2018) suggest that the arcuate shape of the Pamir margin may have been inherited. Paleomagnetic data also indicates that the degree of counterclockwise rotation decreases significantly towards the northwest, away from the Pamir mountain front (Bourgeois et al., 1997). Related to this issue is the question of whether a proximal Alai Basin was subducted beneath the northern Pamir margin (Sobel et al., 2013) or if it was uplifted and eroded during exhumation of the northern Pamir (Chapman et al., 2017). Future studies are needed to help resolve these questions and to understand the complex interplay between basin and orogen dynamics in the Pamir region.

6 | SUMMARY AND CONCLUSIONS

The Tajik Basin is a long-lived basin closely linked to changing tectonic regimes in the Pamir orogenic system. Detrital zircon U–Pb, detrital ZFT, sandstone petrography and conglomerate composition suggest that the Pamir Mountains were the primary source of sediment to the Tajik Basin from Cretaceous time onwards. The Tajik Basin received sediment from terranes located progressively father into the Pamir hinterland through time. Terranes in the north Pamir, like the Karakul–Mazar subduction–accretion complex, were dominant sources of sediment during the Early to mid-Cretaceous. Sediment derived from the Central Pamir terrane was first deposited into the basin during the Late Cretaceous to early Paleogene, and sediment sourced from the South Pamir terrane was deposited during the Miocene. The most significant change in provenance occurs at the base of the Baldshuan Formation (across a middle Eocene to lower Oligocene disconformity) with large shifts in detrital zircon U–Pb and detrital ZFT age populations.

The Tajik Basin is a composite basin system that was constructed by three main basin-forming episodes (Figure 9). Lower to mid-Cretaceous rocks were deposited in a retroarc foreland basin, associated with low-angle subduction of Tethyan oceanic lithosphere under Asia, the northward migration of continental arc magmatism and crustal shortening within the Pamir. Upper Cretaceous to lower Eocene rocks were deposited in an extensional basin during oceanic slab rollback or foundering beneath the Pamir. The modern foreland basin system initiated during the mid-Eocene and is interpreted as a retro-wedge foreland basin system associated with India–Asia collision. The upper Eocene to lower Oligocene disconformity in the Tajik Basin is interpreted to record the passage of a flexural forebulge.

The results of this study suggest that long-lived sedimentary basins in retrowedge positions may record plate margin processes that are far removed from the active depositional system (e.g. Horton & Fuentes, 2016). These basins can be investigated to constrain the timing and the type of subduction-related processes that regulate orogenic growth.

ACKNOWLEDGEMENTS

Support was provided by NSF EAR-1450899 (B.C.), the American Philosophical Society (J.C.), the American Association of Petroleum Geologists (J.C.), the Geological Society of America (J.C.) and Exxon Mobil Corporation (B.C.). Comments by editor Nadine McQuarrie, Lin Li, Ed Sobel and an anonymous reviewer significantly improved the manuscript.

DATA AVAILABILITY

The data that support the findings of this study are openly available in the supplementary material.

ORCID

James B. Chapman https://orcid.org/0000-0002-1145-4687

REFERENCES

Alsharhan, A. S., & Kendall, C. S. C. (2003). Holocene coastal carbonates and evaporites of the southern Arabian Gulf and their ancient analogues. *Earth-Science Reviews*, *61*, 191–243. https://doi.org/10.1016/S0012-8252(02)00110-1

Angiolini, L., Zanchi, A., Zanchetta, S., Nicora, A., & Vezzoli, G. (2013). The Cimmerian geopuzzle: New data from South Pamir. *Terra Nova*, *25*, 352–360. https://doi.org/10.1111/ter.12042

Beaumont, C. (1981). Foreland basins. *Geophysical Journal International*, *65*, 291–329. https://doi.org/10.1111/j.1365-246X.1981.tb02715.x

Blayney, T., Dupont-Nivet, G., Najman, Y., Proust, J. N., Meijer, N., Roperch, P., … Guo, Z. (2019). Tectonic evolution of the Pamir Recorded in the Western Tarim Basin (China): Sedimentologic and magnetostratigraphic analyses of the Aertashi section. *Tectonics*, *38*, 492–515. https://doi.org/10.1029/2018TC005146

Boothroyd, J. C., & Ashley, G. M. (1975). Processes, bar morphology, and sedimentary structures on braided outwash fans, northeastern Gulf of Alaska. In A. V. Jopling & B. C. McDonald (Eds.), *Glaciofluvial and Glaciolacustrine Sedimentation*, (pp. 193–222). Broken Arrow, Ok, USA: SEPM Special Publication

Bosboom, R., Dupont-Nivet, G., Grothe, A., Brinkhuis, H., Villa, G., Mandic, O., … Krijgsman, W. (2013). Linking Tarim Basin sea retreat (west China) and Asian aridification in the late Eocene. *Basin Research*, *26*, 621–640. https://doi.org/10.1111/bre.12054

Bosboom, R., Mandic, O., Dupont-Nivet, G., Proust, J. N., Ormukov, C., & Aminov, J. (2017). Late Eocene palaeogeography of the proto-Paratethys Sea in Central Asia (NW China, southern Kyrgyzstan and SW Tajikistan). *Geological Society, London, Special Publications*, *427*, 565–588. https://doi.org/10.1144/SP427.11

Boulin, J. (1988). Hercynian and Eocimmerian events in Afghanistan and adjoining regions. *Tectonophysics*, *148*, 253–278. https://doi.org/10.1016/0040-1951(88)90134-5

Bourgeois, O., Cobbold, P. R., Rouby, D., Thomas, J. C., & Shein, V. (1997). Least squares restoration of Tertiary thrust sheets in map view, Tajik depression, central Asia. *Journal of Geophysical Research: Solid Earth*, *102*, 27553–27573. https://doi.org/10.1029/97JB02477

Bown, T. M., & Kraus, M. J. (1987). Integration of channel and floodplain suites, I. Developmental sequence and lateral relations of alluvial paleosols. *Journal of Sedimentary Research*, *57*, 587–601.

Bratash, V. I., Egupov, S. V., Pechnikov, V. V., & Shelomentsev, A. I. (1970). *The geology and petroleum potential of northern Afghanistan* (288 pp.). Moscow, Russia: Nedra.

Brookfield, M. E., & Hashmat, A. (2001). The geology and petroleum potential of the North Afghan platform and adjacent areas (northern Afghanistan, with parts of southern Turkmenistan, Uzbekistan and Tajikistan). *Earth-Science Reviews*, *55*, 41–71. https://doi.org/10.1016/S0012-8252(01)00036-8

Burg, J. P. (2011). The Asia–Kohistan–India collision: Review and discussion. In D. Brown & P. D. Ryan (Eds.), *Arc-continent collision* (pp. 279–309). Berlin, Germany: Springer.

Burtman, V. S. (2000). Cenozoic crustal shortening between the Pamir and Tien Shan and a reconstruction of the Pamir-Tien Shan transition zone for the Cretaceous and Palaeogene. *Tectonophysics*, *319*, 69–92. https://doi.org/10.1016/S0040-1951(00)00022-6

Burtman, V. S., & Molnar, P. H. (1993). *Geological and geophysical evidence for deep subduction of continental crust beneath the Pamir*. Boulder, Co, USA: Geological Society of America, Special Publication v. 281, 76p.

Carrapa, B., DeCelles, P. G., Wang, X., Clementz, M. T., Mancin, N., Stoica, M., … Chen, F. (2015). Tectono-climatic implications of Eocene Paratethys regression in the Tajik basin of central Asia. *Earth and Planetary Science Letters*, *424*, 168–178. https://doi.org/10.1016/j.epsl.2015.05.034

Carrapa, B., Mustapha, F. S., Cosca, M., Gehrels, G., Schoenbohm, L. M., Sobel, E. R., … Goodman, P. (2014). Multisystem dating of modern river detritus from Tajikistan and China: Implications for crustal evolution and exhumation of the Pamir. *Lithosphere*, *6*, 443–455. https://doi.org/10.1130/L360.1

Chapman, J. B., Carrapa, B., Ballato, P., DeCelles, P. G., Worthington, J., Oimahmadov, I., … Ketcham, R. (2017). Intracontinental subduction beneath the Pamir Mountains: Constraints from thermokinematic modeling of shortening in the Tajik fold-and-thrust belt. *GSA Bulletin*, *129*, 1450–1471.

Chapman, J. B., Robinson, A. C., Carrapa, B., Villarreal, D., Worthington, J., DeCelles, P., … Gehrels, G. (2018). Cretaceous shortening and exhumation history of the South Pamir terrane. *Lithosphere*, *10*, 494–511. https://doi.org/10.1130/L691.1

Chapman, J. B., Scoggin, S. H., Kapp, P., Carrapa, B., Ducea, M. N., Worthington, J., … Gadoev, M. (2018). Mesozoic to Cenozoic magmatic history of the Pamir. *Earth and Planetary Science Letters*, *482*, 181–192. https://doi.org/10.1016/j.epsl.2017.10.041

Chatelain, J. L., Roecker, S. W., Hatzfeld, D., & Molnar, P. (1980). Microearthquake seismicity and fault plane solutions in the Hindu Kush region and their tectonic implications. *Journal of Geophysical Research: Solid Earth*, *85*, 1365–1387. https://doi.org/10.1029/JB085iB03p01365

Chen, X., Chen, H., Lin, X., Cheng, X., Yang, R., Ding, W., … Zhang, Y. (2018). Arcuate Pamir in the Paleogene? Insights from a review of stratigraphy and sedimentology of the basin fills in the foreland of NE Chinese Pamir, western Tarim Basin: Earth Science Reviews, *180*, 1–16.

Coutand, I., Strecker, M. R., Arrowsmith, J. R., Hilley, G., Thiede, R. C., Korjenkov, A., ... Omuraliev, M. (2002). Late Cenozoic tectonic development of the intramontane Alai Valley, (Pamir-Tien Shan region, central Asia): An example of intracontinental deformation due to the Indo-Eurasia collision: Tectonics, v. 21, n. 6. https://doi.org/10.1029/2002TC001358

Cowgill, E. (2010). Cenozoic right-slip faulting along the eastern margin of the Pamir salient, northwestern China. *Geological Society of America Bulletin*, *122*, 145–161. https://doi.org/10.1130/B26520.1

Crampton, S. L., & Allen, P. A. (1995). Recognition of forebulge unconformities associated with early stage foreland basin development: Example from the North Alpine Foreland Basin. *AAPG Bulletin*, *79*, 1495–1514. https://doi.org/10.1306/7834DA1C-1721-11D7-8645000102C1865D

Dalrymple, R. W., Zaitlin, B. A., & Boyd, R. (1992). Estuarine facies models: Conceptual basis and stratigraphic implications. *Journal of Sedimentary Research*, *62*, 1130–1146. https://doi.org/10.1306/D4267A69-2B26-11D7-8648000102C1865D

Davidzon, R. M., Kreidenkov, G. P., & Salibaev, G. K. (1982). Stratigraphy of paleogene deposits of the Tajik depression and adjacent areas (119 pp.). Dushanbe, Tajikistan: Donish.

De Grave, J., Glorie, S., Ryabinin, A., Zhimulev, F., Buslov, M. M., Izmer, A., … Van den haute, P. (2012). Late Palaeozoic and Meso-Cenozoic tectonic evolution of the southern Kyrgyz Tien Shan: Constraints from multi-method thermochronology in the Trans-Alai, Turkestan-Alai segment and the southeastern Ferghana Basin. *Journal of Asian Earth Sciences*, *44*, 149–168. https://doi.org/10.1016/j.jseaes.2011.04.019

De Pelsmaeker, E., Jolivet, M., Laborde, A., Poujol, M., Robin, C., Zhimulev, F. I., … De Grave, J. (2018). Source-to-sink dynamics in the Kyrgyz Tien Shan from the Jurassic to the Paleogene: Insights from sedimentological and detrital zircon U-Pb analyses. *Gondwana Research*, *54*, 180–204. https://doi.org/10.1016/j.gr.2017.09.004

Debon, F., & Ali-Khan, N. (1996). Alkaline orogenic plutonism in the Karakorum batholith: The Upper Cretaceous KozSar complex

(Karambar valley, N. Pakistan). *Geodinamica Acta*, *9*, 145–160. https://doi.org/10.1080/09853111.1996.11105282

DeCelles, P. G. (2012). Foreland basin systems revisited: Variations in response to tectonic settings. In C. Busby & A. Azor, (Eds.), *Tectonics of sedimentary basins: Recent advances* (pp. 405–426). Oxford, UK: Wiley-Blackwell

DeCelles, P. G., & DeCelles, P. C. (2001). Rates of shortening, propagation, underthrusting, and flexural wave migration in continental orogenic systems. *Geology*, *29*, 135–138. https://doi.org/10.1130/0091-7613(2001)029<0135:ROSPUA>2.0.CO;2

DeCelles, P. G., & Giles, K. A. (1996). Foreland basin systems. *Basin Research*, *8*(2), 105–123.

DeCelles, P. G., Gray, M. B., Ridgway, K. D., Cole, R. B., Pivnik, D. A., Pequera, N., & Srivastava, P. (1991). Controls on synorogenic alluvial-fan architecture, Beartooth Conglomerate (Palaeocene), Wyoming and Montana. *Sedimentology*, *38*, 567–590. https://doi.org/10.1111/j.1365-3091.1991.tb01009.x

DeCelles, P. G., Kapp, P., Gehrels, G. E., & Ding, L. (2014). Paleocene-Eocene foreland basin evolution in the Himalaya of southern Tibet and Nepal: Implications for the age of initial India-Asia collision. *Tectonics*, *33*, 824–849. https://doi.org/10.1002/2014TC003522

Dewey, J. F. (1982). Plate tectonics and the evolution of the British Isles: Thirty-fifth William Smith Lecture. *Journal of the Geological Society*, *139*, 371–412. https://doi.org/10.1144/gsjgs.139.4.0371

Dickinson, W. R. (1985). Interpreting provenance relations from detrital modes of sandstones. In G. G. Zuffa, (Ed.), *Provenance of arenites* (pp. 333–361). Dordrecht: Springer.

Ding, L., Qasim, M., Jadoon, I. A., Khan, M. A., Xu, Q., Cai, F., … Yue, Y. (2016). The India-Asia collision in north Pakistan: Insight from the U-Pb detrital zircon provenance of Cenozoic foreland basin. *Earth and Planetary Science Letters*, *455*, 49–61. https://doi.org/10.1016/j.epsl.2016.09.003

Djalilov, M. R. (1971). *Stratigraphy of Upper Cretaceous deposits of the Tadjik Depression*. Dushanbe, Tajikistan: Donish (in Russian).

Filonov, A. I., & Koroly, A. N. (1966). *Explanatory Note for the Geological Map, Sheet J-42-XVI*. Moscow, Russia: Nedra (in Russian).

Fürsich, F. T., Brunet, M. F., Auxiètre, J. L., & Munsch, H. (2017). Lower-Middle Jurassic facies patterns in the NW Afghan-Tajik Basin of southern Uzbekistan and their geodynamic context. *Geological Society, London, Special Publications*, *427*, 357–409. https://doi.org/10.1144/SP427.9

Garzanti, E., Doglioni, C., Vezzoli, G., & Ando, S. (2007). Orogenic belts and orogenic sediment provenance. *The Journal of Geology*, *115*, 315–334. https://doi.org/10.1086/512755

Hacker, B. R., Ratschbacher, L., Rutte, D., Stearns, M. A., Malz, N., Stübner, K., … Everson, A. (2017). Building the Pamir-Tibet Plateau-Crustal stacking, extensional collapse, and lateral extrusion in the Pamir: 3. Thermobarometry and petrochronology of deep Asian crust. *Tectonics*, *36*(9), 1743–1766.

Hamburger, M. W., Sarewitz, D. R., Pavlis, T. L., & Popandopulo, G. A. (1992). Structural and seismic evidence for intracontinental subduction in the Peter the First Range, central Asia. *Geological Society of America Bulletin*, *104*, 397–408. https://doi.org/10.1130/0016-7606(1992)104<0397:SASEFI>2.3.CO;2

Handford, C. R. (1981). Coastal sabkha and salt pan deposition of the lower Clear Fork Formation (Permian), Texas. *Journal of Sedimentary Research*, *51*, 761–778. https://doi.org/10.1306/212F7DA1-2B24-11D7-8648000102C1865D

Hart, B. S., & Plint, A. G. (1995). Gravelly shoreface and beachface deposits. In A. G. Plint (Ed.), *Sedimentary facies analysis: A tribute to the research and teaching of Harold G. Reading* (pp. 75–99). Blackwell, Oxford, UK: Special publication v. 22.

Hein, F. J., & Walker, R. G. (1977). Bar evolution and development of stratification in the gravelly, braided, Kicking Horse River, British Columbia. *Canadian Journal of Earth Sciences*, *14*, 562–570. https://doi.org/10.1139/e77-058

Horton, B. K., & Fuentes, F. (2016). Sedimentary record of plate coupling and decoupling during growth of the Andes. *Geology*, *44*, 647–650. https://doi.org/10.1130/G37918.1

Ingersoll, R. V. (1990). Actualistic sandstone petrofacies: Discriminating modern and ancient source rocks. *Geology*, *18*, 733–736. https://doi.org/10.1130/0091-7613(1990)018<0733:ASPDMA>2.3.CO;2

Ingersoll, R. V. (2012). Tectonics of sedimentary basins, with revised nomenclature. In C. J. Busby & A. Azor (Eds.), *Tectonics of sedimentary basins, recent advances* (pp. 1–43). Oxford, UK: Wiley-Blackwell.

Jepson, G., Glorie, S., Konopelko, D., Gillespie, J., Danišík, M., Evans, N. J., … Collins, A. S. (2018). Thermochronological insights into the structural contact between the Tian Shan and Pamirs, Tajikistan. *Terra Nova*, *30*, 95–104. https://doi.org/10.1111/ter.12313

Jiang, Y. H., Liu, Z., Jia, R. Y., Liao, S. Y., Zhou, Q., & Zhao, P. (2012). Miocene potassic granite–syenite association in western Tibetan Plateau: Implications for shoshonitic and high Ba–Sr granite genesis. *Lithos*, *134*, 146–162. https://doi.org/10.1016/j.lithos.2011.12.012

Käßner, A., Ratschbacher, L., Pfänder, J. A., Hacker, B. R., Zack, G., Sonntag, B. L., … Oimahmadov, I. (2016). Proterozoic-Mesozoic history of the Central Asian orogenic belt in the Tajik and southwestern Kyrgyz Tian Shan: U-Pb, 40Ar/39Ar, and fission-track geochronology and geochemistry of granitoids. *Geological Society of America Bulletin*, *129*, 281–303.

Kaya, M. Y., Dupont-Nivet, G., Proust, J. N., Roperch, P., Bougeois, L., Meijer, N., … Barbolini, N. (2019). Paleogene evolution and demise of the proto-Paratethys Sea in Central Asia (Tarim and Tajik basins): Role of intensified tectonic activity at ca. 41 Ma. *Basin Research*, *31*, 461–486.

Keen, M. (1978). The Tertiary—Palaeogene. In R. H. Bate & E, Robinson (Eds.), *A Stratigraphical Index of British Ostracoda, British Micropalaeontological Society Special Publication, v. 1* (pp. 385–449). Liverpool, UK: Seel House Press.

Kendall, C. G. S. C. (1968). Recent algal mats of a Persian Gulf lagoon. *SEPM Journal of Sedimentary Research*, *38*, 1040–1058. https://doi.org/10.1306/74D71AF5-2B21-11D7-8648000102C1865D

Klocke, M., Voigt, T., Kley, J., Pfeifer, S., Rocktäschel, T., Keil, S., & Gaupp, R. (2017). Cenozoic evolution of the Pamir and Tien Shan Mountains reflected in syntectonic deposits of the Tajik Basin: Geological Society. *London, Special Publications*, *427*, 523–564. https://doi.org/10.1144/SP427.7

Leith, W. (1982). Rock assemblages in central Asia and the evolution of the southern Asian margin. *Tectonics*, *1*, 303–318. https://doi.org/10.1029/TC001i003p00303

Leith, W. (1985). A mid-Mesozoic extension across Central Asia? *Nature*, *313*, 567–570. https://doi.org/10.1038/313567a0

Li, T., Chen, J., Thompson, J. A., Burbank, D. W., & Xiao, W. (2012). Equivalency of geologic and geodetic rates in contractional orogens: New insights from the Pamir Frontal thrust. *Geophysical Research Letters*, *39*(15), L15305. https://doi.org/10.1029/2012GL051782

Liu, D., Li, H., Sun, Z., Cao, Y., Wang, L., Pan, J., … Ye, X. (2017). Cenozoic episodic uplift and kinematic evolution between the Pamir and southwestern Tien Shan. *Tectonophysics*, *712-713*, 438–454. https://doi.org/10.1016/j.tecto.2017.06.009

Lukens, C. E., Carrapa, B., Singer, B. S., & Gehrels, G. (2012). Miocene exhumation of the Pamir revealed by detrital geothermochronology of Tajik rivers. *Tectonics*, *31*, TC2014. https://doi.org/10.1029/2011TC003040

Mack, G. H., James, W. C., and Monger, H. C. (1993). Classification of paleosols. *Geological Society of America Bulletin*, *105*, 129–136. https://doi.org/10.1130/0016-7606(1993)105<0129:COP>2.3.CO;2

McBride, E. F. (1963). A classification of common sandstones. *Journal of Sedimentary Research*, *33,* 664–669. https://doi.org/10.1306/74D70EE8-2B21-11D7-8648000102C1865D

McKenzie, D. (1978). Some remarks on the development of sedimentary basins. *Earth and Planetary Science Letters*, *40*, 25–32. https://doi.org/10.1016/0012-821X(78)90071-7

McNutt, M. K., Diament, M., & Kogan, M. G. (1988). Variations of elastic plate thickness at continental thrust belts. *Journal of Geophysical Research*, *93*, 8825–8838. https://doi.org/10.1029/JB093iB08p08825

Miall, A. D. (1977). A review of the braided-river depositional environment. *Earth-Science Reviews*, *13*, 1–62. https://doi.org/10.1016/0012-8252(77)90055-1

Miall, A. D. (1996). *The geology of fluvial deposits: Sedimentary facies, basin analysis, and petroleum geology* (582 p.). New York, NY: Springer Publishing.

Muftiev, Z. Z., & Shachnev, A. S. (1967). *Explanatory note for the geological map, sheet J-42-X*. Moscow, Russia: Nedra (in Russian).

Najman, Y., Jenks, D., Godin, L., Boudagher-Fadel, M., Millar, I., Garzanti, E., … Bracciali, L. (2017). The Tethyan Himalayan detrital record shows that India-Asia terminal collision occurred by 54 Ma in the Western Himalaya. *Earth and Planetary Science Letters*, *459*, 301–310. https://doi.org/10.1016/j.epsl.2016.11.036

Naylor, M., & Sinclair, H. D. (2008). Pro-vs. retro-foreland basins. *Basin Research*, *20*(3), 285–303. https://doi.org/10.1111/j.1365-2117.2008.00366.x

Nikolaev, V. G. (2002). Afghan-Tajik depression: Architecture of sedimentary cover and evolution. *Russian Journal of Earth Sciences*, *4*, 399–421. https://doi.org/10.2205/2002ES000106

Reineck, H. E., & Singh, I. B. (1980). Tidal flats. In *Depositional sedimentary environments* (pp. 430–456). Berlin, Germany: Springer.

Reineck, H. E., & Wunderlich, F. (1968). Classification and origin of flaser and lenticular bedding. *Sedimentology*, *11*, 99–104. https://doi.org/10.1111/j.1365-3091.1968.tb00843.x

Robinson, A. C. (2015). Mesozoic tectonics of the Gondwanan terranes of the Pamir plateau. *Journal of Asian Earth Sciences*, *102*, 170–179. https://doi.org/10.1016/j.jseaes.2014.09.012

Robinson, A. C., Ducea, M., & Lapen, T. J. (2012). Detrital zircon and isotopic constraints on the crustal architecture and tectonic evolution of the northeastern Pamir. *Tectonics*, *31*. https://doi.org/10.1029/2011TC003013

Robinson, A. C., Yin, A., Manning, C. E., Harrison, T. M., Zhang, S.-H., & Wang, X.-F. (2004). Tectonic evolution of the northeastern Pamir: Constraints from the northern portion of the Cenozoic Kongur Shan extensional system. *Geological Society of America Bulletin*, *116*, 953–974.

Robinson, A. C., Yin, A., Manning, C. E., Harrison, T. M., Zhang, S.-H., & Wang, X.-F. (2007). Cenozoic evolution of the eastern Pamir: Implications for strain accommodation mechanisms at the western end of the Himalayan-Tibetan orogen. *Geological Society of America Bulletin*, *119*, 882–896. https://doi.org/10.1130/B25981.1

Rust, B. R. (1972). Structure and process in a braided river. *Sedimentology*, *18*(3–4), 221–245. https://doi.org/10.1111/j.1365-3091.1972.tb00013.x

Rust, B. R. (1978). Depositional models for braided alluvium. In A. D. Miall (Ed.), *Fluvial Sedimentology* (Canadian Society of Petroleum Geologists Memoir 5, pp. 605–625). Cambridge, UK: Cambridge University Press.

Rutte, D., Lothar, R., Schneider, S., Stübner, K., Stearns, M. A., Gulzar, M. A., & Hacker, B. R. (2017). Building the Pamir-Tibet Plateau—Crustal Stacking, Extensional Collapse, and Lateral Extrusion in the Central Pamir: 1. Geometry and Kinematics. *Tectonics*, *36*, 342–384.

Schmalholz, M. (2004). *The amalgamation of the Pamirs and their subsequent evolution in the far field of the India-Asia collision* (PhD thesis, 103 p.). Universität Tübingen, Germany.

Schneider, F. M., Yuan, X., Schurr, B., Mechie, J., Sippl, C., Haberland, C., … Negmatullaev, S. (2013). Seismic imaging of subducting continental lower crust beneath the Pamir. *Earth and Planetary Science Letters*, *375*, 101–112. https://doi.org/10.1016/j.epsl.2013.05.015

Schwab, M., Ratschbacher, L., Siebel, W., McWilliams, M., Minaev, V., Lutkov, V., … Wooden, J. L. (2004). Assembly of the Pamirs: Age and origin of magmatic belts from the southern Tien Shan to the southern Pamirs and their relation to Tibet. *Tectonics*, *23*(4), 31.

Sclater, J. G., & Christie, P. A. (1980). Continental stretching: An explanation of the post-Mid-Cretaceous subsidence of the central North Sea Basin. *Journal of Geophysical Research: Solid Earth*, *85*, 3711–3739. https://doi.org/10.1029/JB085iB07p03711

Sengor, A. C. (1984). The Cimmeride orogenic system and the tectonics of Eurasia. *Geological Society of America Special Paper*, *195*, 181–241.

Simakov, S. N. (1952). *Cretaceous deposits of the Buhara-Tadjik area*. Leningrad: VNIGRI (in Russian).

Simonov, V. A., Mikolaichuk, A. V., Safonova, I. Y., Kotlyarov, A. V., & Kovyazin, S. V. (2015). Late Paleozoic-Cenozoic intra-plate continental basaltic magmatism of the Tienshan–Junggar region in the SW Central Asian Orogenic Belt. *Gondwana Research*, *27*, 1646–1666. https://doi.org/10.1016/j.gr.2014.03.001

Sinclair, H. D., Coakley, B. J., Allen, P. A., & Watts, A. B. (1991). Simulation of foreland basin stratigraphy using a diffusion model of mountain belt uplift and erosion: An example from the central Alps, Switzerland. *Tectonics*, *10*, 599–620. https://doi.org/10.1029/90TC02507

Sippl, C., Schurr, B., Yuan, X., Mechie, J., Schneider, F. M., Gadoev, M., … Radjabov, N. (2013). Geometry of the Pamir-Hindu Kush intermediate-depth earthquake zone from local seismic data. *Journal of Geophysical Research: Solid Earth*, *118*, 1438–1457. https://doi.org/10.1002/jgrb.50128

Smit, M. A., Ratschbacher, L., Kooijman, E., & Stearns, M. A. (2014). Early evolution of the Pamir deep crust from Lu-Hf and U-Pb geochronology and garnet thermometry. *Geology*, *42*, 1047–1050. https://doi.org/10.1130/G35878.1

Smith, S. A. (1990). The sedimentology and accretionary styles of an ancient gravel-bed stream: The Budleigh Salterton Pebble Beds

(Lower Triassic), southwest England. *Sedimentary Geology*, *67*, 199–219. https://doi.org/10.1016/0037-0738(90)90035-R

Sobel, E. R. (1999). Basin analysis of the Jurassic-Lower Cretaceous southwest Tarim basin, northwest China. *Geological Society of America Bulletin*, *111*, 709–724. https://doi.org/10.1130/0016-7606(1999)111<0709:BAOTJL>2.3.CO;2

Sobel, E. R., & Arnaud, N. (2000). Cretaceous–Paleogene basaltic rocks of the Tuyon basin, NW China and the Kyrgyz Tian Shan: the trace of a small plume. *Lithos*, *50*, 191–215. https://doi.org/10.1016/S0024-4937(99)00046-8

Sobel, E. R., Chen, J., Schoenbohm, L. M., Thiede, R., Stockli, D. F., Sudo, M., & Strecker, M. R. (2013). Oceanic-style subduction controls late Cenozoic deformation of the Northern Pamir orogeny. *Earth and Planetary Science Letters*, *363*, 204–218. https://doi.org/10.1016/j.epsl.2012.12.009

Stearns, M. A., Hacker, B. R., Ratschbacher, L., Rutte, D., & Kylander-Clark, A. R. C. (2015). Titanite petrochronology of the Pamir gneiss domes: Implications for middle to deep crust exhumation and titanite closure to Pb and Zr diffusion. *Tectonics*, *34*, 784–802. https://doi.org/10.1002/2014TC003774

Steckler, M. S., & Watts, A. B. (1978). Subsidence of the Atlantic-type continental margin off New York. *Earth and Planetary Science Letters*, *41*, 1–13.

Swift, D. J., Hudelson, P. M., Brenner, R. L., & Thompson, P. (1987). Shelf construction in a foreland basin: Storm beds, shelf sandbodies, and shelf-slope depositional sequences in the Upper Cretaceous Mesaverde Group, Book Cliffs, Utah. *Sedimentology*, *34*, 423–457. https://doi.org/10.1111/j.1365-3091.1987.tb00578.x

Tapponnier, P., Mattauer, M., Proust, F., & Cassaigneau, C. (1981). Mesozoic ophiolites, sutures, and large-scale tectonic movements in Afghanistan. *Earth and Planetary Science Letters*, *52*, 355–371.

Tevelev, A. V., & Georgievskii, B. V. (2012). Deformation history and hydrocarbon potential of the Southwestern Gissar Range (Southern Uzbekistan). *Moscow University Geology Bulletin*, *67*(6), 340–352. https://doi.org/10.3103/S0145875212060075

Thomas, J. C., Chauvin, A., Gapias, D., Bazhenov, M. L., Perroud, H., Cobbold, P. R., & Burtman, V. S. (1994). Paleomagnetic evidence for Cenozoic block rotations in the Tadjik depression. *Central Asia: Journal Geophysical Research: Solid Earth*, *99*, 15141–15160. https://doi.org/10.1029/94JB00901

Ulmishek, G. F. (2004) Petroleum geology and resources of the Amu-Darya basin, Turkmenistan, Uzbekistan, Afghanistan, and Iran. Iran: US Department of the Interior, US Geological Survey.

Van Hinte, J. E. (1978). Geohistory analysis–application of micropaleontology in exploration geology. *AAPG Bulletin*, *62*, 201–222. https://doi.org/10.1306/C1EA4815-16C9-11D7-8645000102C1865D

Varban, B. L., & Plint, A. G. (2008). Palaeoenvironments, palaeogeography, and physiography of a large, shallow, muddy ramp: Late Cenomanian-Turonian Kaskapau Formation, Western Canada foreland basin. *Sedimentology*, *55*, 201–233. https://doi.org/10.1111/j.1365-3091.2007.00902.x

Varentsov, M. I., Aleshina, Z. I., & Kornienko, G. E. (1977). Tectonics and petroleum potential of the Tajik depression (108 p). Moscow, Russia: Nauka.

Vlasov, N. G., Pyzhjanov, I. P., & Loziev, V. P. (1964). *Explanatory note for the geological map, sheet J-42-XVII*. Moscow, Russia: Nedra (in Russian).

Vlasov, N., Yu, G., Dyakov, A., & Cherev, E. S. (1991). *Geological map of the Tajik SSR and adjacent territories, 1:500,000*. Saint Petersburg: Vsesojuznoi Geologic Institute of Leningrad.

Wang, Y., Feng, R., & Hsu, H. (1997), Lithospheric isostasy, Flexure and Strength of Upper Mantle in Tibetan Plateau. In H. Dawei (Ed.), *Structure of the Lithosphere and Deep Processes: Proceedings of the 30th International Geological Congress, VSP, Netherlands* (Vol. *4*, pp. 153–160).

White, N., & McKenzie, D. (1988). Formation of the "steer's head" geometry of sedimentary basins by differential stretching of the crust and mantle. *Geology*, *16*, 250–253. https://doi.org/10.1130/0091-7613(1988)016<0250:FOTSSH>2.3.CO;2

Worthington, J. R., Kapp, P., Minaev, V., Chapman, J. B., Mazdab, F. K., Ducea, M. N., … Gadoev, M. (2017). Birth, life, and demise of the Andean-syn-collisional Gissar arc: Late Paleozoic tectono-magmatic-metamorphic evolution of the southwestern Tian Shan, Tajikistan. *Tectonics*, *36*, 1861–1912.

Wright, V. P. (1984). Peritidal carbonate facies models: A review. *Geological Journal*, *19*, 309–325. https://doi.org/10.1002/gj.3350190402

Xiao, W. J., Windley, B. F., Chen, H. L., Zhang, G. C., & Li, J. L. (2002). Carboniferous-Triassic subduction and accretion in the western Kunlun, China: Implications for the collisional and accretionary tectonics of the northern Tibetan Plateau. *Geology*, *30*, 295–298. https://doi.org/10.1130/0091-7613(2002)030<0295:CTSAAI>2.0.CO;2

Xie, X., & Heller, P. L. (2009). Plate tectonics and basin subsidence history. *Geological Society of America Bulletin*, *121*, 55–64.

Zonenshain, L. P. (1990). Geology of the USSR: A plate-tectonic synthesis. *American Geophysical Union, Geodynamic Series*, *21*, 242p.

Zonenshain, L. P., & Le Pichon, X. (1986). Deep basins of the Black Sea and Caspian Sea as remnants of Mesozoic back-arc basins. *Tectonophysics*, *123*, 181–211. https://doi.org/10.1016/0040-1951(86)90197-6

SUPPORTING INFORMATION

Additional supporting information may be found online in the Supporting Information section at the end of the article.

How to cite this article: Chapman JB, Carrapa B, DeCelles PG, et al. The Tajik Basin: A composite record of sedimentary basin evolution in response to tectonics in the Pamir. *Basin Res*. 2019;00:1–21. https://doi.org/10.1111/bre.12381